Journal of Shellfish Research, Vol. 42, No. 2, 177–197, 2023.

BATHYMODIOLAMIDES C, D, AND E, NECROSIS INDUCERS FROM A DEEP-SEA HYDROTHERMAL VENT INVERTEBRATE MUSSEL, *BATHYMODIOLUS AZORICUS*

ERIC H. ANDRIANASOLO,[1,2]* LITI HARAMATY,[3] KERRY L. MCPHAIL[4] AND RICHARD A. LUTZ[3]

[1]*Centre National de Recherches Industrielle et Technologique (CNRIT), 38, rue Rasamimanana, Fiadanana, Antananarivo, 101, Madagascar;* [2]*University of Waterloo, Biology Department, 200 University Ave W, Waterloo, Ontario, N2L3G1, Canada;* [3]*Department of Marine and Coastal Sciences, Rutgers, The State University of New Jersey, 71 Dudley Road, New Brunswick, NJ 08901-8521, USA;* [4]*Department of Pharmaceutical Sciences, Oregon State University, 103 SW Memorial Place, Corvallis, OR 97331, USA*

ABSTRACT Three ceramides with intriguing structural features, bathymodiolamides C (**1**), D (**2**), and E (**3**), were isolated from the deep-sea hydrothermal vent invertebrate mussel *Bathymodiolus azoricus* that inhabits vent environments along the Mid-Atlantic Ridge. The molecular structures of these compounds were elucidated using a combination of Nuclear Magnetic Resonance spectroscopy, mass spectrometry, and chemical degradation. Biological activities were assessed by Lactate Dehydrogenase assay for necrosis induction and the patented ApopScreen cell-based screen for apoptosis-induction and potential anticancer activity. This represents a second report of ceramide natural products from *B. azoricus*.

KEY WORDS: Ceramide, necrosis inducer, anticancer agent, marine biotechnology, marine hydrothermal vent mussel, *Bathymodiolus azoricus*

INTRODUCTION

Cell death regulations have been arranged based on morphological criteria into three categories (Okada & Mak 2004): apoptosis, autophagy, and necrosis. Apoptosis or type I cell death (the most widely investigated) is expressed by cell rounding, membrane blebbing, cytoplasmic condensation and fragmentation, nuclear pyknosis, and chromatin condensation/fragmentation. Apoptotic bodies are rapidly phagocytized and absorbed by macrophages or neighboring cells (Lauber et al. 2004). Type II cell death occurs with autophagy, which is expressed by the appearance of abundant autophagic vacuoles in the cytoplasm, and expansion of the endoplasmic reticulum and the Golgi apparatus (Cuervo 2004, Rodriguez-Enriquez et al. 2004). Necrosis, or type III cell death, was considered as an unregulated and uncontrollable process, although evidence now reveals that necrosis can also be regulated (Vanden Berghe et al. 2010). Triggering the programmed necrosis ("necroptosis") by death receptors (such as tumor necrosis factor receptor 1) requires the kinase activity of receptor-interacting protein 1 (RIP1; also known as RIPK1) and RIP3 (also known as RIPK3), and its execution involves the active disintegration of mitochondrial, lysosomal, and plasma membranes. Necroptosis engages in the pathogenesis of diseases, including ischemic injury, neurodegeneration, and viral infection, thereby representing an attractive target for the avoidance of unwarranted cell death (Vandenabeele et al. 2010).

The vast oceanic ecosystem holds enormous, potential for drug discovery. Within this large ecosystem, one area remains particularly enigmatic: deep-sea hydrothermal vents, which are distinguished by high concentrations of reduced sulfur compounds (Gartner et al. 2008). Life is sustained by the growth of chemolithoautotrophic bacteria capable of oxidizing hydrogen sulfide, hydrogen, and other reduced inorganic compounds to construct energy that is used to fuel carbon dioxide fixation into macromolecules. Dual symbiosis furnishes a clear nutritional advantage to bathymodiolin mussels, allowing them to obtain energy from both sulfide and methane at the vent sites (Nelson et al. 1995). Along the Mid-Atlantic Ridge in the vicinity of the Azores, *Bathymodiolus azoricus* inhabits vent sites with unusual levels of heavy metals, pH, temperature, CO_2, methane, and sulfide while thriving successfully with environmental microbes (Bettencourt et al. 2007).

Andrianasolo et al. (2011) previously reported the isolation and structure elucidation of bathymodiolamides A and B, ceramide derivatives from *Bathymodiolus azoricus* (mistakenly identified in the initial report as the marine hydrothermal vent mussel *Bathymodiolus thermophilus* [Andrianasolo et al. 2011]), in continuing efforts to study, discover, and develop new marine natural product biomedicines. The present paper reports the isolation of new bathymodiolides C, D, and E from *B. azoricus*, together with reisolation of bathymodiolamides A and B. These metabolites, and additional congeners F and G, which are not presented here, are the subject of a US patent (Lutz et al. 2020). Ceramide natural products have been reported recently from the deep-sea fungus *Acremonium alternatum* (Li et al. 2022), and from the Far Eastern deep-sea starfish *Ceramaster patagonicus* (Malyarenko et al. 2022). Ceramides from marine organisms possess diverse anticancer, antibacterial, and antiviral, including anti-COVID-19 bioactivities (Abdelhameed et al. 2020, Abdelkarem et al. 2020, Eltamany et al. 2021, Lei et al. 2021, Malyarenko et al. 2021, Sallam et al. 2021, Elhady et al. 2022, Kawahara & Yokota 2022, Kawahara et al. 2021, Singh & Tilvi 2022).

MATERIALS AND METHODS

General Experimental Procedures: The optical rotations were recorded using JASCO P 1010 polarimeter. UV and FT-IR spectra were measured using Hewlett-Packard 8/r52A and Nicolet 510 instruments, respectively. Nuclear Magnetic Resonance (NMR) spectra were recorded using Bruker 600 MHz instrument. The residual solvent resonances at $\delta_{H/C}$ 3.31/49.15

*Corresponding author. E-mail: eric.andrianasolo@uwaterloo.ca
DOI: 10.2983/035.042.0201

(CD_3OD) were used for spectral references. ESIMS data were acquired on a Waters Micromass LCT Classic mass spectrometer and a Varian 500-MS LC ion trap instrument. An ABI-MDS SCIEX 4800 instrument was used to record MALDITOFMS data. High Performance Liquid Chromatography (HPLC) separations of bathymodiolamides were performed using Waters 510 HPLC pumps, a Waters 717 plus autosampler, and a Waters 996 photodiode array detector, utilizing HPLC grade solvents.

Animal Material: The Deep Submergence Vehicle (DSV) Alvin was used to collect *Bathymodiolus azoricus* from an active hydrothermal vent along the Mid-Atlantic Ridge (Region: North, Location: Lucky Strike [LS], Dive Number: 3118, Date: July 08, 1997, Latitude: 37° 17.36′ N, Longitude: 32° 16.75′ W, Depth: 1,731 m). The identification of the organisms was performed by Dr. R. C. Vrijenhoek (Department of Marine and Coastal Sciences, Rutgers, The State University of New Jersey) and Dr. C. Vetriani (Department of Biochemistry and Microbiology, Rutgers, The State University of New Jersey). A voucher specimen is available at the Center for Deep-Sea Ecology and Biotechnology, Department of Marine and Coastal Sciences, Rutgers, The State University of New Jersey, New Brunswick, NJ 08,901 with collection number AD-MUS-LS-7/8/97.

Extraction and Isolation: Using methanol as a solvent for extraction, *Bathymodiolus azoricus* tissue (100 g wet mass) was repeatedly extracted with MeOH to give a polar organic extract (850 mg). A portion of this extract (20 mg) was tested for cytotoxicity and induction of apoptosis and was found active. Consequently, the remaining organic extract was fractionated using solid-phase extraction on normal-phase silica to give four fractions, F1–F4. The fractions were respectively eluted with hexanes, hexanes-EtOH, EtOH, and MeOH solvents of increasing degree of polarity. The MeOH fraction (F4) possessed cytotoxicity activity. This fraction was further chromatographed by analytical Reverse Phase HPLC (Phenomenex Luna C_{18}, 250 × 4.60 mm, isocratic elution 4:1 MeOH–H_2O, flow rate 1 mL/min) to yield 11.4 mg of bathymodiolamide A (t_R = 11.5 min), 8.7 mg of bathymodiolamide B (t_R = 9.5 min), 5.5 mg of bathymodiolamide C (**1**) (t_R = 8.5 min), 4 mg of bathymodiolamide D (**2**) (t_R = 12.5 min), and 5 mg of bathymodiolamide E (**3**) (t_R = 10 min).

Bathymodiolamide C (**1**): $[\alpha]^{24}_D$ + 10.2 (c 0.08, MeOH); IR υ_{max} max (neat) 3,350, 3,250, 2,900, 2,850, 1,640, 1,450, 1,050 cm^{-1}; ^1H and ^{13}C NMR, Table 1 and appendix; HRMALDITOFMS *m/z* 1,054.8998 $[M + H]^+$ (calcd for $C_{66}H_{120}NO_8$, 1,054.9008).

Bathymodiolamide D (**2**): $[\alpha]^{24}_D$ + 10.4 (*c* 0.08, MeOH); IR υ_{max} (neat) 3,350, 3,250, 2,900, 2,850, 1,640, 1,450, 1,050 cm^{-1}; ^1H NMR and ^{13}C NMR, Table 2 and appendix; HRMALDITOFMS *m/z* 780.6340 $[M + H]^+$ (calcd for $C_{46}H_{86}NO_8$, 780.6348).

Bathymodiolamide E (**3**): $[\alpha]^{24}_D$ + 10.1 (*c* 0.08, MeOH); IR υ_{max} (neat) 3,350, 3,250, 2,900, 2,850, 1,640, 1,450, 1,050 cm^{-1}; ^1H NMR and ^{13}C NMR, Table 3 and appendix; HRMALDITOFMS *m/z* 1,080.8408 $[M + Na]^+$ (calcd for $C_{64}H_{115}NNaO_{10}$, 1,080.8413).

Lactate Dehydrogenase (LDH) Assay: Bathymodiolamides C (**1**) and E (**2**) were dissolved in DMSO in 5 mM stock. Hydrogen peroxide (H_2O_2) was obtained from EMD Millipore (Catalog #M1072980250). Pierce LDH Cytotoxicity Assay Kit was obtained from Thermo Scientific (Catalog # 88,953). MCF7 human breast cancer cell line was obtained from American Type Culture Collection (Manassas, VA). MCF7 cells were grown in EMEM medium supplemented with 10% heat-inactivated fetal bovine serum, 10 µg/mL bovine insulin, 100 µg/mL of penicillin, and 100 µg/mL of streptomycin. Cultures were maintained at 37 °C in a humidified atmosphere of 5% CO_2 and 95% air.

Lactate Dehydrogenase assay procedure:

(1) 20,000 MCF7 cells/well in 100 µL of 10% FBS culture medium in triplicate wells were seeded in a 96-well plate in an incubator at 37°C, 5% CO_2 for overnight incubation.
(2) The next day, the culture medium was replaced with fresh medium containing 1% FBS medium.
(3) Five doses of bathymodiolamide C (**1**) or E (**3**) at 10, 50, 100, 150, or 200 µM, 0.1% H_2O_2, or 4% DMSO were added to the triplicate wells containing cells and incubated at 37°C, 5% CO_2 for 3 h.
(4) 10 µL of 10× lysis buffer was added to triplicate wells containing cells and incubated at 37°C, 5% CO_2 for 45 min.
(5) 50 µL of each sample medium were transferred to a 96-well flat-bottom plate in triplicate wells.
(6) 50 µL of the assay kit reaction mixture was transferred to each sample well and mixed by gentle shaking.
(7) The plate was incubated at room temperature for 30 min protected from light.
(8) The absorbance at 492 nm was measured immediately using an Envision 2104 Multilabel Reader (PerkinElmer, Santa Clara, CA).
(9) The LDH release (%) was calculated using the formula:

Lactate Dehydrogenase release (%) = (Compound treated sample LDH activity − DMSO treated sample LDH activity) × 100/(10 × Lysis buffer treated sample LDH activity − DMSO treated sample LDH activity)

(10) The LDH release histogram graphs were plotted using the GraphPad Prism 4 program.

Biological Evaluation (Apoptosis Induction): Testing for induction of apoptosis in the presence of bathymodiolamides was carried out as described in Andrianasolo et al. (2007) using the ApopScreen assay. In this assay, the viability of treated W2 (apoptosis competent) and D3 (apoptosis defective) cells is measured using a modification of the MTT assay. For the current study, viability was measured at 0 and 48 h and differential growth was calculated in the presence and absence of the compounds. Staurosporine (an apoptosis inducer) was used as a positive control and DMSO as a negative control.

Cytotoxicity Assay: Two cancer cell lines were used to demonstrate the inhibitory effect on cell growth of bathymodiolamides. Cells were treated with varying concentrations of compounds and the IC_{50} values were calculated. All compounds were shown to kill or inhibit the growth of HeLa and MCF7 cancer cell lines.

Acid and Base Hydrolysis: Dissolution of bathymodiolamides **1**, **2**, and **3** was achieved in MeOH (1.5 mL), followed by addition of NaOMe (2.5 mg). The mixture was stirred for 3 h at room temperature. The reaction mixture was then quenched using the acidic ion-exchange resin Amberlite IRC-50 (Rohm and Hass, H + form) followed by filtration to remove the resin. The drying of the filtrate was achieved under reduced pressure. The dried filtrate was partitioned between $CHCl_3$ and H_2O. The organic layer was analyzed by GC-MS with SPB-5 Capillary GC Column.

Enzymatic Hydrolysis: Dissolutions of bathymodiolamides **1, 2**, and **3** (2 mg) were achieved separately in 4 mL of dioxane-H_2O (1:1). With steady shaking for 4 h at 37 °C, the

TABLE 1.

NMR data for bathymodiolamide C (1) at 600 MHz in CD_3OD.

Position				δ_C mult				δ_H, multiplet patterns (*J* in Hz)				HMBC
1-a	–	1-b	–	63.3	–	CH_2	–	4.00, d (4.4)	–	–	4.00, d (4.4)	2, 3
2	–	–	–	53.9	–	CH	–	3.98, dd (4.4, 2)	–	–	–	1, 3, 1′
3	–	–	–	71.4	–	CH	–	4.05, dd (2, 6.4)	–	–	–	2, 4
4	–	–	–	70.6	–	CH	–	5.26, dt (6.4, 3)	–	–	–	3, 5, 1″
5-a	–	5-b	–	61.9	–	CH_2	–	4.19, dd (12, 3)	–	–	4.46, dd (12, 3)	4, 1‴
1′	1″	1‴	1⁗	173.2 qC	173.4 qC	173.8 qC	59.5 CH_2	–	–	–	4.28, m	1, 2⁗
2′	2″	2‴	2⁗	33.3 CH_2	36.1 CH_2	33.3 CH_2	66.3 CH_2	2.36, t (7.5)	2.20, t (7.2)	2.35, t (7.5)	3.65, m	1′, 4′ 1″, 4″ 1‴, 4‴ 1⁗, 3⁗
3′	3″	3‴	3⁗	24.9 CH_2	25.1 CH_2	24.7 CH_2	53.6 CH_3	1.60, bs	1.63, m 1.71, m	1.69, bs	3.23, s	1′, 5′ 1″, 5″ 1‴, 5‴ 2⁗
4′	4″	4‴	–	29.6 CH_2	26.9 CH_2	29.6 CH_2	–	1.32, bs	2.14, m	1.32, bs	–	2′, 6′ 2″, 6″ 2‴, 6‴
5′	5″	5‴	–	29.6 CH_2	129.9 CH_2	29.6 CH_2	–	1.32, bs	5.45, m	1.32, bs	–	3′, 7′ 3″, 7″ 3‴, 7‴
6′	6″	6‴	–	29.6 CH_2	127.6 CH	29.6 CH_2	–	1.32, bs	5.35, m	1.32, bs	–	4′, 8′ 4″, 8″ 4‴, 8‴
7′	7″	7‴	–	29.7 CH_2	25.3 CH_2	29.7 CH_2	–	1.32, bs	2.86, m	1.32, bs	–	5′, 9′ 5″, 9″ 5‴, 9‴
8′	8″	8‴	–	29.7 CH_2	127.5 CH	29.7 CH_2	–	1.32, bs	5.40, m	1.32, bs	–	6′, 10′ 6″, 10″ 6‴, 10‴
9′	9″	9‴	–	29.7 CH_2	129.5 CH	29.7 CH_2	–	1.32, bs	5.36, m	1.32, bs	–	7′, 11′ 7″, 11″ 7‴, 11‴
10′	10″	10‴	–	29.7 CH_2	25.3 CH_2	29.7 CH_2	–	1.32, bs	2.85, m	1.32, bs	–	8′, 12′ 8″, 12″ 8‴, 12‴
11′	11″	11‴	–	29.5 CH_2	129.5 CH	29.5 CH_2	–	1.32, bs	5.39, m	1.32, bs	–	9′, 13′ 9″, 13″ 9‴, 13‴
12′	12″	12‴	–	29.5 CH_3	128.0 CH	29.5 CH_2	–	1.32, bs	5.39, m	1.32, bs	–	10′, 14′ 10″, 14″ 10‴, 14‴
13′	13″	13‴	–	29.5 CH_2	25.3 CH_2	29.5 CH_2	–	1.32, bs	2.84, m	1.32, bs	–	11′, 15′ 11″, 15″ 11‴, 15‴
14′	14″	14‴	–	29.5 CH_2	128.5 CH	29.4 CH_2	–	1.32, bs	5.38, m	1.32, bs	–	12′, 16′ 12″, 16″ 12‴, 16‴
15′	15″	15‴	–	29.5 CH_2	129.2 CH	28.9 CH_2	–	1.32, bs	5.38, m	1.32, bs	–	13′, 17′ 13″, 17″ 13‴, 16‴
16′	16″	16‴	–	29.5 CH_2	25.3 CH_2	13.2 CH_3	–	1.32, bs	2.84, m	0.92, t (7.5)	–	14′, 18′ 14″, 18″ 14‴, 15‴
17′	17″	–	–	29.5 CH_2	129.2 CH	–	–	1.32, bs	5.35, m	–	–	15′, 19′ 15″, 19″
18′	18″	–	–	29.5 CH_2	128.6 CH	–	–	1.32, bs	5.36, m	–	–	16′, 20′ 16″, 20″
19′	19″	–	–	29.5 CH_2	27.4 CH_2	–	–	1.32, bs	–	–	–	17′, 21′ 17″, 21″
20′	20″	–	–	29.0 CH_2	22.6 CH_2	–	–	1.32, bs	2.08, m	–	–	18′, 21′ 18″, 21″
21′	21″	–	–	13.2 CH_3	13.3 CH_3	–	–	0.91, t (7.5)	1.35, m	0.93, t (7.5)	–	19′, 20′ 19″, 20″

TABLE 2.

NMR data for bathymodiolamide D (2) at 600 MHz in CD_3OD.

Position				δ_C mult				δ_H, multiplet patterns (*J* in Hz)				HMBC
1-a	1-b	–	–	63.3 CH_2	–	–	–	4.00, d (4.4)	4.00, d (4.4)	–	–	2, 3
2	–	–	–	53.9 CH	–	–	–	3.98, dd (4.4, 2)	–	–	–	1, 3, 1′
3	–	–	–	71.2 CH	–	–	–	4.05, dd (2, 6.4)	–	–	–	2, 4
4	–	–	–	70.6 CH	–	–	–	5.26, dt (6.4, 3)	–	–	–	3, 5, 1″
5-a	5-b	–	–	61.9 CH_2	–	–	–	4.19, dd (12, 3)	4.46, dd (12, 3)	–	–	4, 1‴
1′	1″	1‴	1⁗	173.2 qC	173.4 qC	173.8 qC	69.5 CH_2	–	–	–	4.28, m	1, 2⁗
2′	2″	2‴	2⁗	30.0 CH_2	30.1 CH_2	30.2 CH_2	66.3 CH_2	2.33, t (7.5)	2.20, t (7.2)	2.33, t (7.5)	3.65, m	1′, 4′ 1″, 4″ 1‴, 4‴ 1⁗, 3⁗
3′	3″	3‴	3⁗	24.9 CH_2	25.5 CH_2	24.6 CH_2	53.6 CH_3	1.60, bs	1.63, m	1.69, bs	3.23, s	1′, 5′ 1″, 5″ 1‴, 5‴ 2‴
4′	4″	4‴	–	29.8 CH_2	31.7 CH_2	29.8 CH_2	–	1.32, bs	2.05, m	1.32, bs	–	2′, 6′ 2″, 6″ 2‴, 6‴
5′	5″	5‴	–	29.8 CH_2	129.5 CH_2	29.8 CH_2	–	1.32, bs	5.38, m	1.32, bs	–	3′, 7′ 3″, 7″ 3‴, 7‴
6′	6″	6‴	–	29.8 CH_2	129.5 CH	29.8 CH_2	–	1.32, bs	5.38, m	1.32, bs	–	4′, 8′ 4″, 8″ 4‴, 8‴
7′	7″	7‴	–	29.7 CH_2	26.5 CH_2	29.7 CH_2	–	1.32, bs	2.81, m	1.32, bs	–	5′, 9′ 5″, 9″ 5‴, 9‴
8′	8″	8‴	–	29.7 CH_2	127.9 CH	29.7 CH_2	–	1.32, bs	5.38, m	1.32, bs	–	6′, 10′ 6″, 10″ 6‴, 10‴
9′	9″	9‴	–	29.5 CH_2	127.9 CH	29.6 CH_2	–	1.32, bs	5.38, m	1.32, bs	–	7′, 11′ 7″, 11″ 7‴, 11‴
10′	10″	10‴	–	29.5 CH_2	26.9 CH_2	29.6 CH_2	–	1.32, bs	2.05, m	1.32, bs	–	8′, 12′ 8″, 12″ 8‴, 12‴
11′	11″	11‴	–	28.9 CH_2	26.5 CH_2	29.5 CH_2	–	1.32, bs	1.40, m	1.32, bs	–	9′, 12′ 10″, 12″ 10‴, 13‴
12′	12″	12‴	–	13.2 CH_3	13.1 CH_3	29.5 CH_2	–	0.89, t (7.0)	0.91, t (7.5)	1.32, bs	–	10′, 11′ 10″, 11″ 11‴, 13‴
–	–	13‴	–	–	–	28.9 CH_2	–	–	–	1.32, bs	–	12‴, 14‴
–	–	14‴	–	–	–	13.0 CH_3	–	–	–	0.90, t (7.5)	–	12‴, 13‴

TABLE 3.

NMR data for bathymodiolamide E (3) at 600 MHz in CD_3OD.

Position				δ_C mult				δ_H, multiplet patterns (*J* in Hz)				HMBC
1-a	1-b	–	–	63.3 CH_2	4.00, d (4.4)	–	–	4.00, d (4.4)	–	–	–	2, 3
2	–	–	–	53.9 CH	–	–	–	3.98, dd (4.4, 2)	–	–	–	1, 3, 1′
3	–	–	–	71.4 CH	–	–	–	4.05, dd (2, 6.4)	–	–	–	2, 4
4	–	–	–	70.6 CH	–	–	–	5.26, dt (6.4, 3)	–	–	–	3, 5, 1″
5-a	5-b	–	–	61.9 CH_2	–	–	–	4.19, dd (12, 3)	4.46, dd (12, 3)	–	–	4, 1‴
1′	1″	1‴	1⁗	173.2 qC	173.4 qC	173.8 qC	59.5 CH_2	–	–	4.28, m	–	–
2′	2″	2‴	2⁗	33.6 CH_2	36.1 CH_2	24.3 CH_2	66.3 CH_2	2.35, t (7.5) 2.20, t (7.2)	1.98, m	2.00, m	3.65, m	1′, 4′ 1″, 4″ 1‴, 4‴
3′	3″	3‴	3⁗	26.7 CH_2	36.2 CH_2	35.4 CH	60.9 CH_2	1.58, m	2.18, m	3.14, m	3.71, d(6)	1′, 5′ 1″, 5″ 1‴, 5‴
4′	4″	4‴	4⁗	29.6 CH_2	129.5 CH	71.7 CH	60.9 CH_2	1.32, bs	5.38, m	4.07, m	3.71, d(6)	2′, 6′ 2″, 6″ 2‴, 6‴ 5⁗
5′	5″	5‴	5⁗	29.6 CH_2	127.6 CH	129.6 CH	53.4 CH_3	1.32, bs	5.38, m	5.48, dd (18, 6)	3.25, s	3′, 7′ 3″, 7″ 3‴, 7‴ 4⁗
6′	6″	6‴	–	29.6 CH_2	25.3 CH_2	133.5 CH	–	1.32, bs	2.88, m	5.71, dd (18, 6)	–	4′, 8′ 4″, 8″ 4‴, 8⁗
7′	7″	7‴	–	29.7 CH_2	127.6 CH	32.1 CH_2	–	1.32, bs	5.38, m	2.08, m	–	5′, 9′ 5″, 9″ 5‴, 9⁗
8′	8″	8‴	–	29.7 CH_2	129.5 CH	29.7 CH_2	–	1.32, bs	5.38, m	1.32, bs	–	6′, 10′ 6″, 10″ 6‴, 10⁗
9′	9″	9‴	–	29.7 CH_2	25.3 CH_2	29.6 CH_2	–	1.32, bs	2.86, m	1.32, bs	–	7′, 11′ 7″, 11″ 7‴, 11⁗
10′	10″	10‴	–	29.7 CH_2	128.1 CH	29.6 CH_2	–	1.32, bs	5.38, m	1.32, bs	–	8′, 12′ 8″, 12″ 8‴, 12⁗
11′	11″	11‴	–	29.5 CH_2	128.0 CH	29.5 CH_2	–	1.32, bs	5.38, m	1.32, bs	–	9′, 12′ 9″, 13″ 9‴, 13⁗
12′	12″	12‴	–	29.5 CH_2	25.3 CH_2	29.5 CH_2	–	1.32, bs	2.84, m	1.32, bs	–	10′, 11′ 10″, 14″ 10‴, 14⁗
13′	13″	13‴	–	29.5 CH_2	128.4 CH	29.5 CH_2	–	1.32, bs	5.38, m	1.32, bs	–	11′, 12′ 11″, 15″ 11‴, 15⁗
14′	14″	14‴	–	29.5 CH_2	129.2 CH	29.4 CH_2	–	1.32, bs	5.38, m	1.32, bs	–	13′, 15′ 12″, 16″ 12‴, 16⁗
15′	15″	15‴	–	29.5 CH_2	27.5 CH_2	28.9 CH_2	–	1.32, bs	2.08, m	1.32, bs	–	14′, 16′ 13″, 16″ 13‴, 16⁗
16′	16″	16‴	–	29.5 CH_2	22.6 CH_2	13.0 CH_3	–	1.32, bs	1.35, m	0.90, t (7.5)	–	15′, 17′ 14″, 15″ 14‴, 15⁗
17′	17″	–	–	29.5 CH_2	13.1 CH_3	–	–	1.32, bs	–	0.91, t (7.5)	–	16′, 18′ 15′, 16′
18′	–	–	–	29.5 CH_2	–	–	–	1.32, bs	–	–	–	17′, 19′
19′	–	–	–	29.5 CH_2	–	–	–	1.32, bs	–	–	–	18′, 20′
20′	–	–	–	29.0 CH_2	–	–	–	1.32, bs	–	–	–	19′, 21′
21′	–	–	–	13.2 CH_3	–	–	–	0.91, t (7.5)	–	–	–	20′, 19′

dissolved bathymodiolamides were treated with lipase enzyme type III (2 mg, 50 unit, from a *Pseudomonas* species, Sigma-Aldrich). Each reaction mixture was quenched with 5% AcOH (1 mL), and the ensuing product was dried under reduced pressure. The resulting crude residues were each dissolved in H_2O and extracted with EtOAc, concentrated under reduced pressure, and analyzed by ESIMS.

RESULTS AND DISCUSSION

Results

Structure Elucidation

Bathymodiolamide C (1). Bathymodiolamide C (**1**) was found to have a molecular formula of $C_{66}H_{119}NO_8$ based on HRMALDITOFMS (*m/z* 1,054.8998 $[M + H]^+$). The resemblance of its ^1H NMR spectrum (Table 1) to those for bathymodiolamides A and B (Andrianasolo et al. 2011) suggested that their structural features are very similar. A noticeable difference between the spectra was the presence of two 2H multiplet at δ_H 3.65 and δ_H 4.28 in the spectrum for **1**.

Analyses of multiplicity edited HSQC and COSY for **1** revealed that the two ^1H signals at δ_H 3.65 and 4.28 belonged to two adjacent methylene groups with ^{13}C shifts characteristic of oxygen bearing carbons (δ_C 66.3 and 59.5, respectively). HMBC correlations revealed a methoxy group attached to the downfield methylene carbon (δ_C 66.3) and an ether bridge from the other methylene (δ_C 59.5) to C-1. This suggested a methoxy ethylene group attached to C-1 by an ether bond in **1**. Following a regioselective enzymic hydrolysis of **1** with lipase enzyme type III in dioxane/H_2O (1:1) at 37 °C for 4 h, only hexadecanoic acid was obtained, as established by comparison with an authentic sample using ESIMS analysis. Thus, it was deduced that the hexadecanoyl residue is attached to the C-5 hydroxyl of **1**. The methanolysis of **1** revealed the presence of heneicosapentaenoic acid methyl ester and docosanoic acid methyl ester as well as hexadecanoic acid methyl ester. The heneicosanoyl moiety was assigned as the C-2 amide by MALDITOFMS/MS, which yielded *m/z* 325.3563 ($[M + 2H]^+$) corresponding to cleavage of this moiety. The remaining heneicosapentaenoyl substituent was then esterified at oxymethine C-4. The structure of **1** is similar to bathymodiolamides A and B with heneicosapentaenoyl and hexadecanoyl residues at C-4 and C-5, respectively. Since bis-allylic ^{13}C NMR signals for Z and E isomers are observed at ca. δ_C 27 and 32 ppm, respectively (Scribe et al. 1988, Ishii et al. 2006), the δ_C 25.3 ppm shift suggested an *all-cis*-5, 8, 11, 14, and 17-heneicosapentaenoyl ester at C-4. The planar structure of bathymodiolamide C (**1**) is established as shown in Figure 1.

Bathymodiolamide D (2). Bathymodiolamide D (**2**) was found to have a molecular formula of $C_{46}H_{85}NO_8$ based on HRMALDITOFMS (*m/z* 780.6340 $[M + H]^+$). ^1H and ^{13}C NMR data (Table 2) for **2** were very close to those for bathymodiolamide B (Andrianasolo et al. 2011), which possesses shorter chain fatty acyl esters than bathymodiolamides A and C (**1**). Multiplicity edited HSQC and COSY correlations revealed signals for two adjacent oxymethylenes at δ_H 3.65/δ_C 66.3 and δ_H 4.28/δ_C 59.5, and HMBC correlations were consistent with a methoxy ethylene group attached to C-1 by an ether bond in **2**, as observed in **1**. Methanolysis of **2** revealed the presence of a dodecadienoic acid methyl ester at C-4, in contrast to the undecadienoic acid methyl ester in bathymodiolamide B. This dodecadienoyl unit was assigned to the C-2 amide on the basis of a tandem mass peak at *m/z* 184.2 $[M + H]^+$. Regioselective enzymic hydrolysis of **2** yielded only tetradecanoic acid, leading to assignment of a tetradecanoyl ester at C-5 position of **2**, as in bathymodiolamide B. The heneicosanoyl moiety was assigned as the C-2 amide by MALDITOFMS/MS, which yielded *m/z* 325.3563 ($[M + 2H]^+$) corresponding to cleavage of this moiety. The remaining heneicosapentaenoyl substituent was then esterified at oxymethine C-4. The structure of **2** is established as shown in Figure 2.

Bathymodiolamide E (3). Bathymodiolamide E (**3**) was found to have a molecular formula of $C_{64}H_{115}NO_{10}$ based on HRMALDITOFMS (*m/z* 1,080.8408 $[M + Na]^+$). The ^1H NMR spectrum (Table 3) for **3** was closely similar to that for bathymodiolamide C (**1**) except for a different distribution of ^1H integrals between the methylene envelope and oxymethylene regions, and two deshielded olefinic COSY-coupled multiplets (δ_H 5.48 and δ_H 5.71). An 18 Hz coupling constant was consistent with a *trans* double bond for these olefinic protons, which were HSQC-correlated to ^{13}C signals at δ_C 129.6 and δ_C 133.6, respectively. The ^1H signal at δ_H 5.48 also displayed a COSY correlation to a 1H oxymethine multiplet at δ_H 4.07, for which the HSQC-correlated ^{13}C shift at δ_C 71.7 was indicative of a hydroxy substituent. Thus, it was concluded that **2** possesses a hydroxy unsaturated fatty acyl moiety. Another striking disparity between the NMR spectra for **1** and **3** was the presence of an additional oxymethylene ^{13}C shift at δ_C 61.0. The latter signal was HSQC-correlated to ^1H multiplets at δ_H 3.71 and 3.65, each of which integrated to 2H. Thus, the ^{13}C signal at δ_C 61.0 represents two oxymethylene carbons. HMBC correlations from δ_H 3.71 and 3.65 correlated to the carbon of the terminal methoxy group at δ_C 53.39. Hence, the structure of **2** has one more ethylene glycol moiety in its structure compared with **1**. The heneicosanoyl moiety was again assigned as the C-2 amide by a tandem MS peak *m/z* 325.3563 ($[M + 2H]^+$)

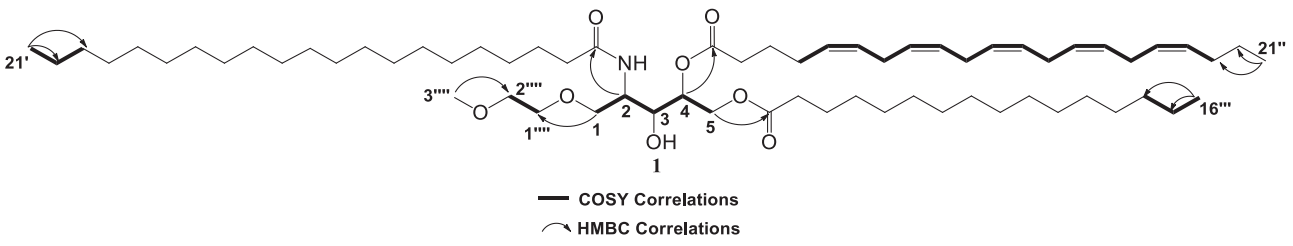

Figure 1. Key HMBC and selected COSY correlations for bathymodiolamide C (1).

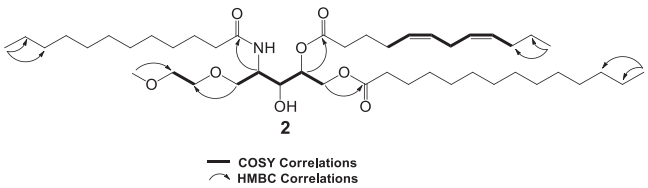

Figure 2. Key HMBC and selected COSY correlations for bathymodiolamide D (2).

corresponding to loss of this moiety from the parent molecule. Regioselective enzymic hydrolysis of **3** yielded 4-hydroxy *trans*-5-hexadecaenoic acid, leading to assignment of a 4-hydroxy *trans*-5-hexadecaenoyl ester at C-5 in **3**. The methanolysis of **3** gave methyl esters of heneicosanoic acid, 4-hydroxy *trans*-5-hexadecaenoic acid and heptadecatetraenoic acid. Consequently, the heptadecatetraenoyl residue is connected to C-4 position in **3**. Bis-allylic carbon signals of heptadecatetraenoyl residue are observed at 25.3 ppm shift suggested that all double bonds of this residue have a cis geometry (Z) (*all-cis*-4, 7, 10, 13-heptadecatetraenoic acid). The planar structure of **3** is established as shown in Figure 3.

Stereochemistry assignment. The coupling constant patterns for the 2-amino-1,3,4,5-pentane tetraol cores in bathymodiolamides A–E were all comparable. As reported previously for bathymodiolamides A and B, the homonuclear coupling constants observed between H-2 and H-3, and H-3 and H-4 are consistent with either (2*S*, 3*S*, 4*R*) or (2*R*, 3*R*, 4*S*) diastereomers. Considering the positive optical rotation values obtained for all bathymodiolamides, they propose an absolute configuration of (2*S*, 3*S*, 4*R*) for bathymodiolamides A–E (Fig. 4), consistent with reported values for D-ribophytosphingosine (lit. $[\alpha]^{25}_{D}$ + 9.5°, *c* 0.5, pyridine; Park et al. [2008]).

Bioactivities

Apoptosis Induction and Cytotoxicity Assay

Bathymodiolamides C (**1**) and E (**3**) were tested with the patented ApopScreen assay to assess their ability to induce apoptosis. In this assay, the D3 cell line is an immortalized epithelial cell line genetically deleted for Bax and Bak. Apoptosis cannot be restored in these cells. W2 cells (wild type) have an intact apoptosis function. W2 and D3 cell lines are used in screening for compounds that promote apoptosis by the criteria of killing W2 and not D3 cells. This screen should identify compounds that have the capacity to activate apoptosis upstream of, and that require Bax and Bak. Both cell lines were tested with bathymodiolamides C (**1**) and E (**3**). A decreased growth rate was measured for D3 cells in the presence of the either compound. Growth of W2 cells was not affected. The results indicate that bathymodiolamides C (**1**) and E (**3**) do not induce apoptosis but may induce a different kind of cell death. Furthermore, the cytotoxicity assay against HeLa ovarian and MCF7 breast cancer cell lines revealed that both compounds kill or inhibit the growth of both cancer cell lines. Since bathymodiolamides did not induce apoptosis, they should induce a nonapoptotic pathway. To verify that assumption, an LDH assay was performed in MCF7 cells.

Lactate Dehydrogenase Assay of Bathymodiolamides C (1) and E (3)

Necrosis leads to the mitochondrial swelling and the augmentation of plasma membrane permeability. The release of LDH, a soluble cytosolic enzyme, into the culture medium after the loss of membrane integrity resulting from necrosis is detectable. Therefore, LDH activity can be detected, measured, and used as an indicator of cell membrane integrity and serves as a general means to assess necrosis.

Results of an LDH assay in MCF7 cells revealed that ceramides **1** and **3** induce necrosis (Figs. 5 and 6).

Co-addition of necrostatin and bathymodiolamides C (**1**) or E (**3**) to Bax and Bak null cells (D3).

To test whether necroptosis was induced in the presence of the compounds, D3 cells were incubated with bathymodiolamides C (**1**, 66 and 132 μg mL^{-1}) and E (**3**, 47 and 95 μg mL^{-1}) with addition of 30 μM necrostatin, a known inhibitor of necroptosis.

In the presence of the each bathymodiolamide alone, cell growth, as compared with the untreated control, was 70% less in the presence of **1**, at both concentrations tested. For **3**, growth was reduced by 70% (95 μg mL-1) and 60% (47 μg mL^{-1}).

Addition of necrostatin to the incubation with each bathymodiolamide resulted in a reduction of 35% in the presence of **1** and 43% in the presence of **3**, compared with untreated control. Thus, necrostatin rescued over 30% of the cells from the negative effect of compound **1**, and 17–27% in the case of **3**. From these results it is evident that bathymodiolamides C (**1**) and E (**3**) have an opposite mode of action compared with necrostatin. Consequently, the assumption that bathymodiolamides kill cancer cells by inducing necrosis is verified.

DISCUSSION

Structure Elucidation

The structural template of bathymodiolamides C–E (**1–3**) is similar to the previously characterized bathymodiolamides A

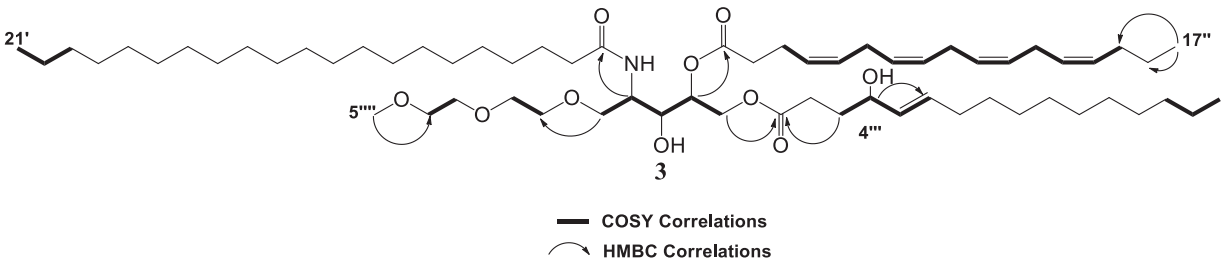

Figure 3. Key HMBC and selected COSY correlations for bathymodiolamide E (3).

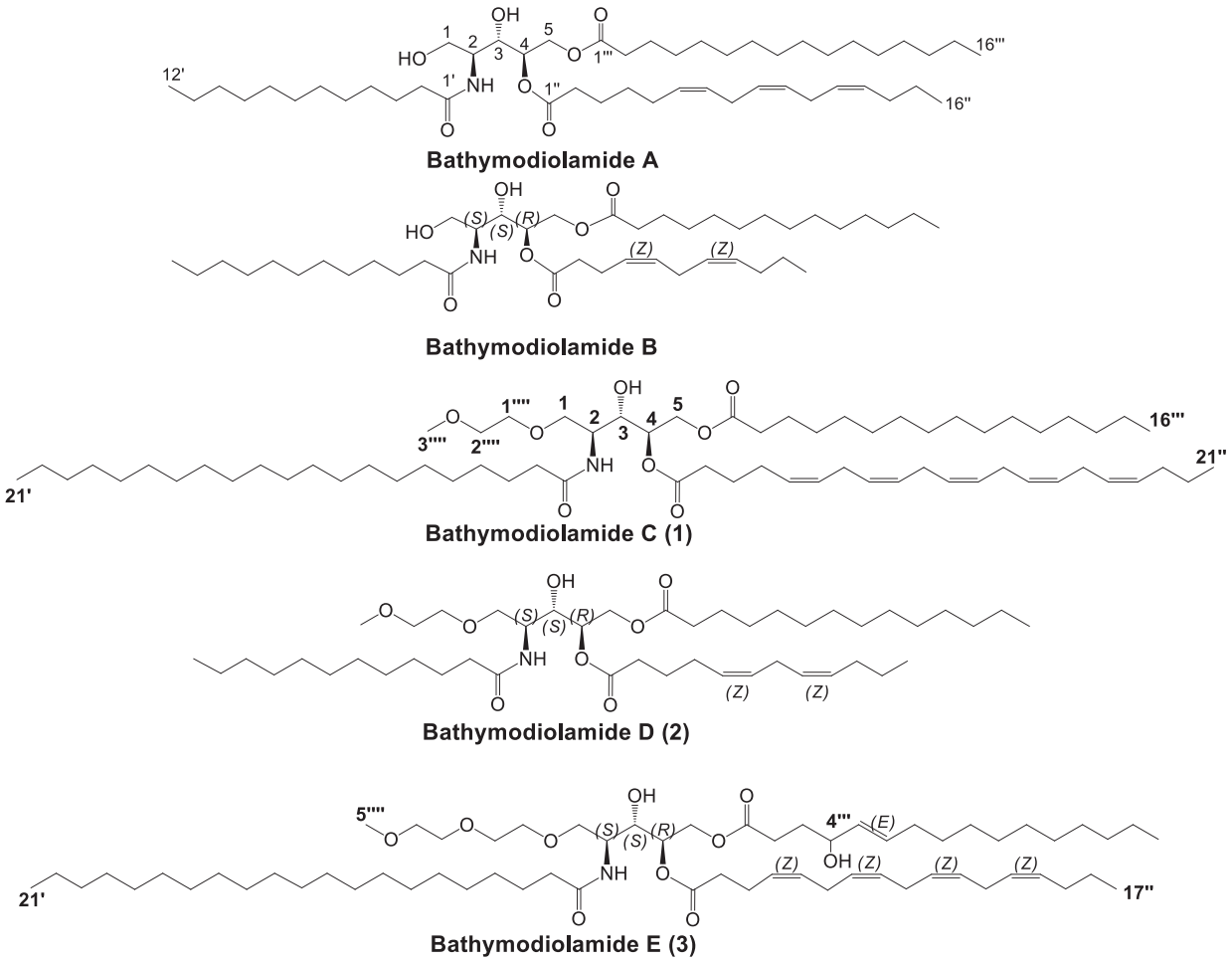

Figure 4. Bathymodiolamides A, B, C (1), D (2), and E (3) drawn according to Park et al. 2008.

and B. The primary difference is the presence of one methoxy ethylene group in bathymodiolamides C (**1**) and D (**2**) and an additional ethylene glycol moiety in bathymodiolamide E (**3**). The relative configuration of the 2-amino-1,3,4,5-pentane tetraol motif is consistent for bathymodiolamides A–E, and as assigned previously for bathymodiolamides A and B (2*S**, 3*S**, 4*R**). The hydroxy bearing C-4‴ chiral center remains unsolved for bathymodiolamide E (**3**). Rigorous assignment of this chiral center requires the synthesis of authentic standards (E)-(4*R*)-4-hydroxyhexadec-5-enoic acid and (E)-(4*S*)-4-hydroxyhexadec-5-enoic acid for comparison with the (E)-4-hydroxyhexadec-5-enoic acid residue of **3**, which is the subject of a future research project. The synthesis of (2*R*, 3*S*, 4*R*) isomers of bathymodiolamides A and B was published in 2021 (Bär et al. 2021). Understandably, the NMR data and coupling constant patterns, as well as the biological activities

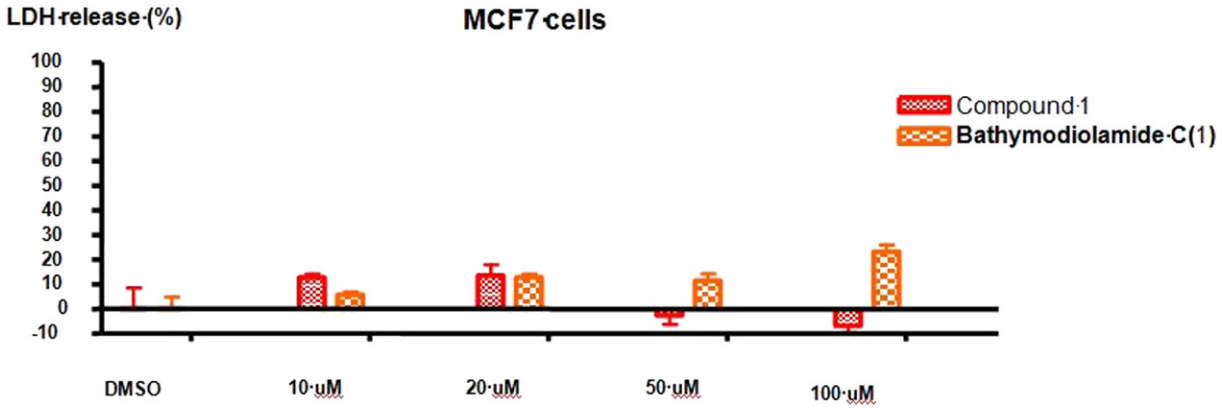

Figure 5. LDH assay results for bathymodiolamide C (1) compared with compound 1: a xenicane diterpene that induces apoptosis and does not show LDH release.

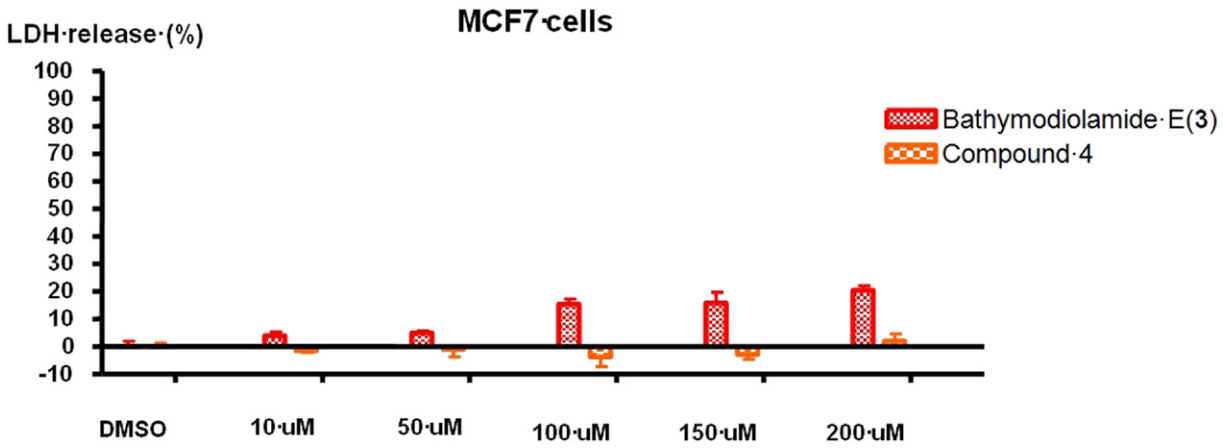

Figure 6. LDH assay results for bathymodiolamide E (3) compared with a compound 4: a xenicane diterpene that induces apoptosis and does not show LDH release).

of the two synthesized compounds are different from the target natural products (bathymodiolamides A and B), as well as bathymodiolamides C–E (**1–3**) reported here. The reported syntheses further confirm that the configuration of the natural products is not (2*R*, 3*S*, 4*R*). Importantly, the choice of (2*R*, 3*S*, 4*R*)-bathymodiolamides A and B as synthetic targets (Bär et al. 2021) likely resulted from their misrepresentation of the (2*S*, 3*S*, 4*R*) configuration in the structures of bathymodiolamides A and B, and typographical misstatement of L-arabinophytosphingosine (2*R*, 3*S*, 4*R*) as a reference standard with the same relative configuration and sign of optical rotation as the natural products. The correct reference standard for their proposed (2*S*, 3*S*, 4*R*) configuration of the bathymodiolamides is D-ribophytosphingosine (Park et al. 2008).

The presence of methoxy ethylene ethers at C-1 for bathymodiolamides C–E (**1–3**) is intriguing and raises concern of artifacts arising during the isolation process. If this were the case, they would expect to isolate bathymodiolamides A and B with their corresponding methoxy ethylene adducts because all of these compounds are subject to the same isolation conditions. Repeated isolations of the bathymodiolamides have never yielded detectable methoxy ethylene adducts of bathymodiolamides A and B. Similarly, they would expect to isolate bathymodiolamides C–E (**1–3**) with the corresponding free hydroxyls, but these have not been detected. Additionally, there is no evidence of bathymodiolamides that are simply methoxylated at C-1. Thus, they conclude that reactions generating artifacts are unlikely and bathymodiolamides C–E (**1–3**) are natural products isolated directly from the deep-sea hydrothermal vent mussel *Bathymodiolus azoricus*.

Bioactivities

Bathymodiolamides did not induce apoptosis but instead induced necrosis. Bathymodiolamides C (**1**) and E (**3**) have the opposite mode of action to necrostatin, a known inhibitor of necroptosis. Most current anticancer drugs kill actively dividing cells by the induction of apoptosis. Unfortunately, cancer cells often acquire resistance to agents that activate the apoptotic pathway, so alternative cell death pathways are important for exploitation in cancer chemotherapy. Bathymodiolamides alone or in combination with other compounds (e.g., with apoptosis inducers) may increase the efficacy of cancer treatments. These new compounds offer new leads and provide promising candidates for anticancer drug research and development.

CONCLUSIONS

This work demonstrated that the deep-sea hydrothermal vent invertebrate mussel *Bathymodiolus azoricus* biosynthesizes bioactive metabolites that may be used for pharmaceutical drug development. Although the structural template of the new bathymodiolamides C, D, and E is related to ceramide, these compounds present interesting structural features, such as the mono or poly ethylene glycol moieties. The biological activities of bathymodiolamides C and E were assessed and revealed that they induce the regulated necrosis pathway or necroptosis. Consequently, these compounds may be useful to complement the action of anticancer drugs when the apoptotic pathway is compromised.

PATENTS

An issued patent is the subject of this work (**United States. Patent Number 10,537,545 B2, January 21, 2020**). Briefly in this patent, the bathymodiolamides, which are necrosis inducers, were combined with apoptosis-inducing xenicane diterpenes to form novel potential anticancer treatments.

FUNDING

This research was funded by Rutgers University through an Academic Excellence award and by NSF grant OCE 03-27373.

DATA AVAILABILITY STATEMENT

Data is available upon reasonable request.

ACKNOWLEDGMENTS

We thank H. Zheng for mass spectrometry analysis at the Center for Advanced Biotechnology and Medicine, Rutgers

University. We also thank the NMR facilities at Oregon State University.

AUTHOR CONTRIBUTIONS

Conceptualization, K.M. and E.A.; methodology, E.A. and L.H.; software, K.M.; validation, E.A., K.M. and R.L.; formal analysis, E.A. and L.H.; investigation, E.A. and R.L.; resources, K.M and E.A.; data curation, E.A.; writing—original draft preparation, E.A.; writing—review and editing, K.M.; visualization, E.A. and K.M; supervision, R.L.; project administration, E.A. and R.L.; funding acquisition, R.L. All authors have read and agreed to the published version of the manuscript.

CONFLICT OF INTEREST

The authors declare no conflict of interest

LITERATURE CITED

Abdelhameed, R. F. A., E. S. Habib, N. A. Eltahawy, H. A. Hassanean, A. K. Ibrahim, A. F. Mohammed, S. Fayez, A. M. Hayallah, K. Yamada, F. A. Behery, M. M. Al-Sanea, S. I. Alzarea, G. Bringmann, S. A. Ahmed & U. R. Abdelmohsen. 2020. New cytotoxic natural products from the red sea sponge *Stylissa carteri*. *Mar. Drugs* 18:241.

Abdelkarem, F. M., E. K. Desoky, A. M. Nafady, A. E. Allam, A. Mahdy, M. Nagata, T. Miyamoto & K. Shimizu. 2020. Isolation of new secondary metabolites from gorgonian soft coral *Heteroxenia fuscescens* collected from Red Sea. *Phytochem. Lett.* 36:156–161.

Andrianasolo, E. H., L. Haramaty, K. Degenhardt, R. Mathew, E. White, R. Lutz & P. Falkowski. 2007. Induction of apoptosis by diterpenes from the soft coral *Xenia elongata. J. Nat. Prod.* 70:1551–1557.

Andrianasolo, E. H., L. Haramaty, K. L. McPhail, E. White, C. Vetriani, P. Falkowski & R. Lutz. 2011. Bathymodiolamides A and B, ceramide derivatives from a deep-sea hydrothermal vent invertebrate mussel, *Bathymodiolus thermophilus. J. Nat. Prod.* 74:842–846.

Bär, A., S. I. Bär, M. Röder & R. Schobert. 2021. Synthesis of the proposed isomers of the deep-sea mussel metabolites bathymodiolamides A and B. *J. Org. Chem.* 86:1868–1873.

Bettencourt, R., P. Roch, S. Stefanni, D. Rosa & A. Colaço. 2007. Deep sea immunity: unveiling immune constituents from the hydrothermal vent mussel *Bathymodiolus azoricus. Mar. Environ. Res.* 64:108–127.

Cuervo, A. M. 2004. Autophagy: many paths to the same end. *Mol. Cell. Biochem.* 263:55–72.

Elhady, S. S., E. S. Habib, R. F. A. Abdelhameed, M. S. Goda, R. M. Hazem, E. T. Mehanna, M. A. Helal, K. M. Hosny, R. M. Diri, H. A. Hassanean, A. K. Ibrahim, E. E. Eltamany, U. A. Abdelmohsen & S. A. Ahmed. 2022. Anticancer effects of new ceramides isolated from the Red Sea red algae *Hypnea musciformis* in a model of Ehrlich ascites carcinoma: LC-HRMS analysis profile and molecular modeling. *Mar. Drugs* 20:63.

Eltamany, E. E., S. S. Elhady, M. S. Goda, O. M. Aly, E. S. Habib, A. K. Ibrahim, H. A. Hassanean, U. R. Abdelmohsen, M. K. Safo & S. A. Ahmed. 2021. Chemical composition of the Red Sea green algae *Ulva lactuca*: isolation and in silico studies of new anti-COVID-19 ceramides. *Metabolites* 11:816.

Gartner, A., J. Wiese & J. F. Imhoff. 2008. Amphritea atlantica gen. nov., sp. nov., a gammaproteobacterium from the Logatchev hydrothermal vent field. *Int. J. Syst. Evol. Microbiol.* 58:34–39.

Ishii, T., T. Okino & Y. Mino. 2006. A ceramide and cerebroside from the starfish *Asterias amurensis* Lütken and their plant-growth promotion activities. *J. Nat. Prod.* 69:1080–1082.

Kawahara, K. & A. Yokota. 2022. Chemical characterization of ceramides isolated from a gliding marine bacterium *Aureispira marina. Biosci. Biotechnol. Biochem.* 86:1136–1143.

Kawahara, K., H. Iida & A. Yokota. 2021. Detection of 2-hydroxy-fatty acids and 2-hydroxy-fatty acid-containing ceramides in a gliding marine bacterium *Aureispira marina*. *J. Gen. Appl. Microbiol.* 67:100–105.

Lauber, K., S. G. Blumenthal, M. Waibel & S. Wesselborg. 2004. Clearance of apoptotic cells: getting rid of the corpses. *Mol. Cell* 14:277–287.

Lei, H., X. Bi, X. Lin, J. She, X. Luo, H. Niu, D. Zhang & B. Yang. 2021. Heterocornols from the sponge-derived fungus *Pestalotiopsis heterocornis* with anti-inflammatory activity. *Mar. Drugs* 19:585.

Li, Y.-H., J. Wu, M.-M. Xie, Y. Zhang & X.-W. Yang. 2022. Chemical constituents of the deep-sea-derived *Acremonium alternatum* and their chemotaxonomic significance. *Biochem. Syst. Ecol.* 103:104443.

Lutz, R., E. Andrianasolo, P. Falkowski, E. White & L. Haramaty. 2020. Ceramide derivatives as anticancer agents United States. Patent Number 10,537,545 B2 January 21.

Malyarenko, T. V., A. A. Kicha, V. A. Stonik & N. V. Ivanchina. 2021. Sphingolipids of asteroidea and holothuroidea: structures and biological activities. *Mar. Drugs* 19:330.

Malyarenko, T. V., V. M. Zakharenko, A. A. Kicha, A. S. Kuzmich, O. S. Malyarenko, A. I. Kalinovsky, R. S. Popov, V. I. Svetashev & N. V. Ivanchina. 2022. New ceramides and cerebrosides from the deep-sea far eastern starfish *Ceramaster patagonicus. Mar. Drugs* 20:641.

Nelson, D. C., K. D. Hagen & D. B. Edwards. 1995. The gill symbiont of a hydrothermal vent mussel, *Bathymodiolus thermophilus*, is a psychrophilic, chemoautotrophic sulfur bacterium. *Mar. Biol.* 121:487–495.

Okada, H. & T. W. Mak. 2004. Pathways of apoptotic and non-apoptotic death in tumour cells. *Nat. Rev. Cancer* 4:592–603.

Park, J., J. H. Lee, Q. Li, K. Diaz, Y. Y.-T. Chang & S. Chung. 2008. Divergent syntheses of all stereoisomers of phytosphingosine and their use in the construction of a ceramide library. *Bioorg. Chem.* 36:220–228.

Rodriguez-Enriquez, S., L. He & J. J. Lemasters. 2004. Role of mitochondrial permeability transition pores in mitochondrial autophagy. *Int. J. Biochem. Cell Biol.* 36:2463–2472.

Sallam, A., M. El-Metwally, M. A. Sabry & M. Elsbaey. 2021. Cladamide: a new ceramide from the endophytic fungus *Cladosporium cladosporioides. Nat. Prod. Res.* 37:1–10.

Scribe, P., J. Guezennec, J. Dagaut, C. Pepe & A. Saliot. 1988. Identification of the position and the stereochemistry of the double bond in monounsaturated fatty acid methyl esters by gas chromatography/mass spectrometry of dimethyl disulfide derivatives. *Anal. Chem.* 60:928–931.

Singh, K. S. & S. Tilvi. 2022. Chemical diversity and bioactivity of marine sponges of the genus *Oceanapia: a review. Mini-Rev. Org. Chem.* 19:66–73.

Vanden Berghe, T., N. Vanlangenakker, E. Parthoens, W. Deckers, M. Devos, N. Festjens, C. J. Guerin, U. T. Brunk, W. Declercq & P. Vandenabeele. 2010. Necroptosis, necrosis and secondary necrosis converge on similar cellular disintegration features. *Cell Death Differ.* 17:922–930.

Vandenabeele, P., L. Galluzzi, T. Vanden Berghe & G. Kroemer. 2010. Molecular mechanisms of necroptosis: an ordered cellular explosion. *Nat. Rev. Mol. Cell Biol.* 11:700–714.

APPENDIX

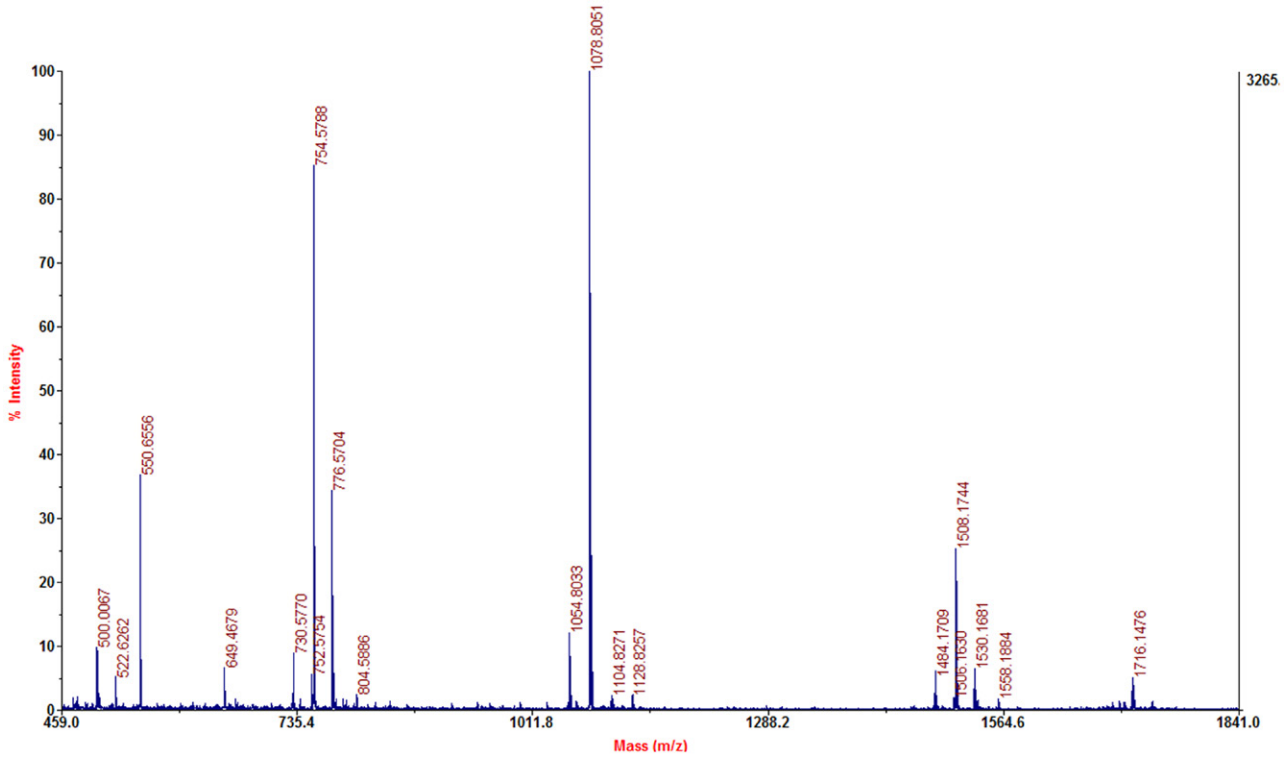

Figure A1. MALDITOFMS of bathymodiolamide C (1).

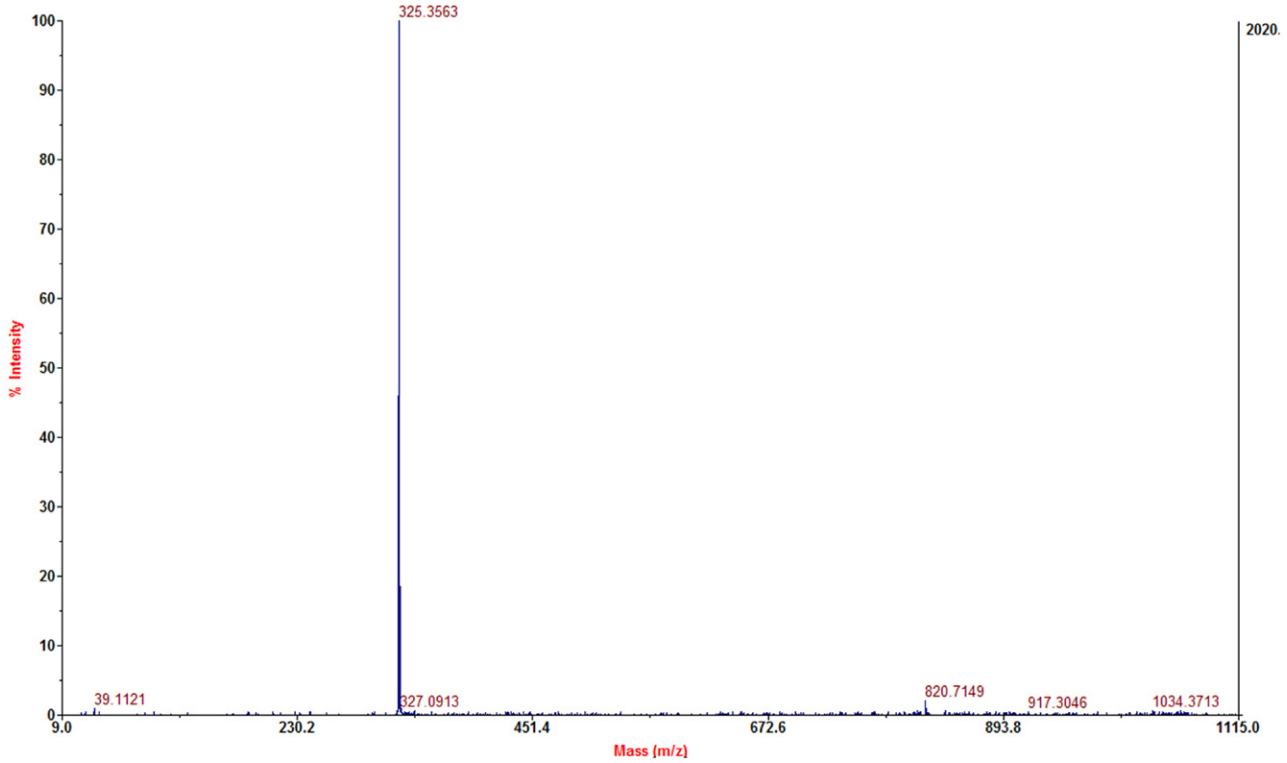

Figure A2. MALDITOFMS/MS of the peak at *m/z* 1,054.8 of bathymodiolamide C (1).

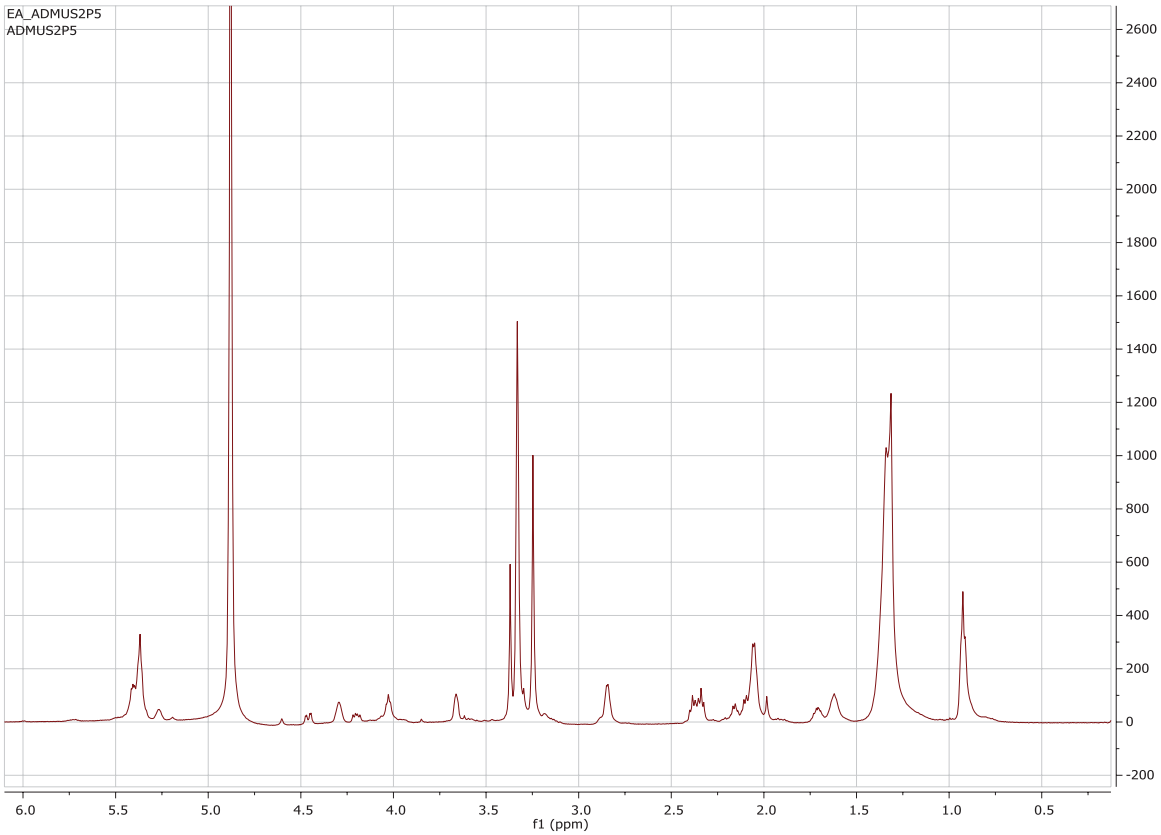

Figure A3. 600 MHz ^{1}H NMR spectrum of bathymodiolamide C (1) in CD_3OD.

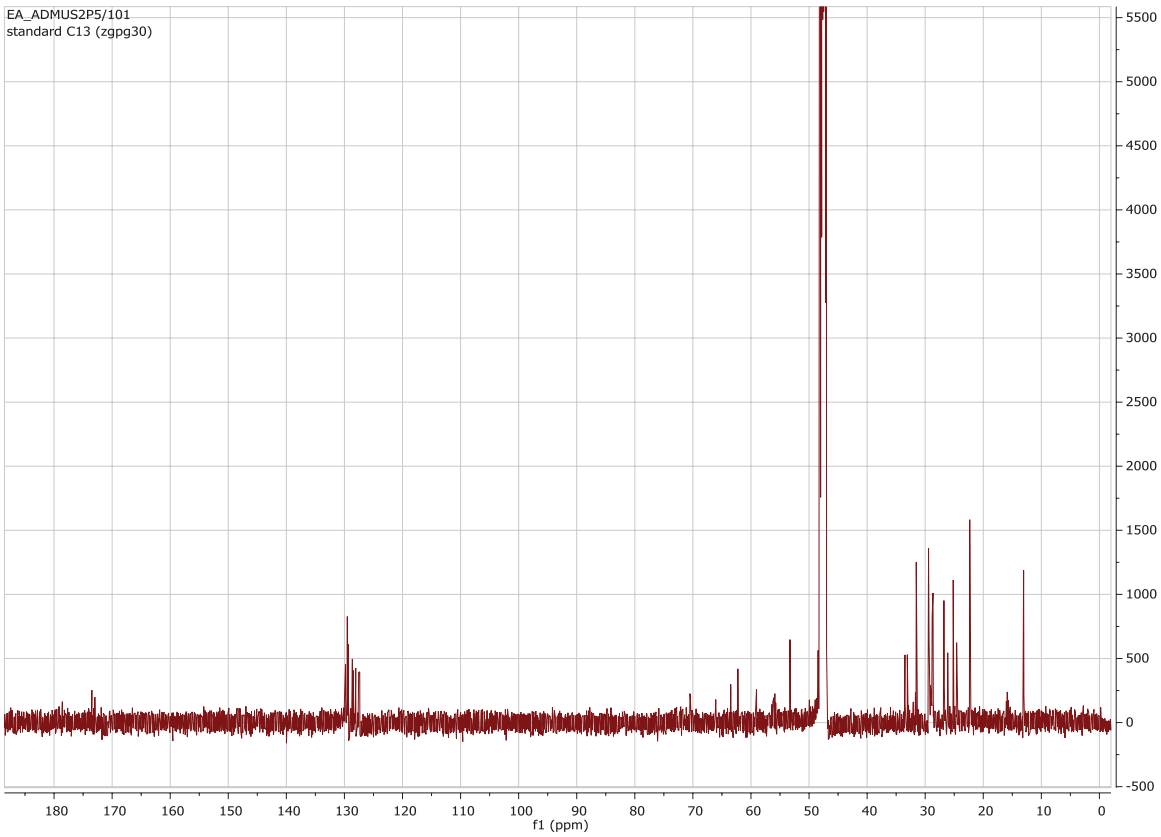

Figure A4. 150 MHz ^{13}C NMR spectrum of bathymodiolamide C (1) in CD_3OD.

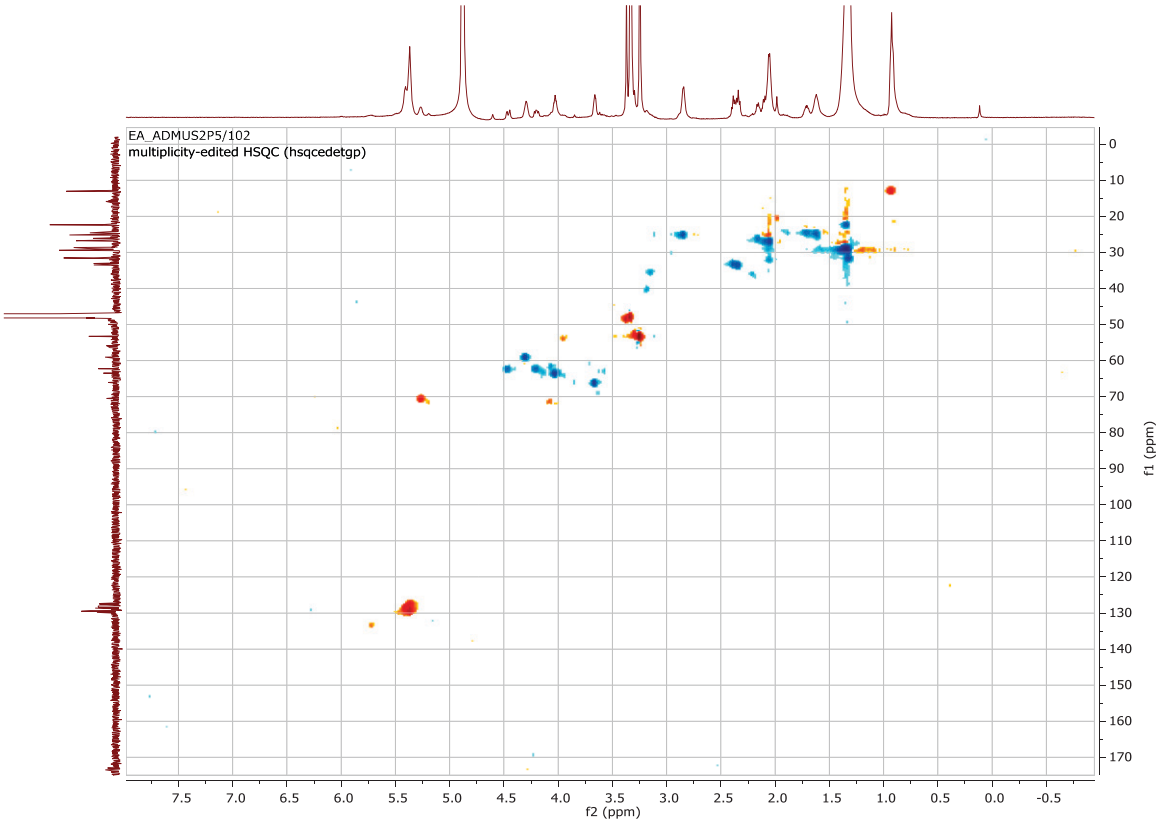

Figure A5. 600 MHz multiplicity edited HSQC spectrum of bathymodiolamide C (1) in CD_3OD.

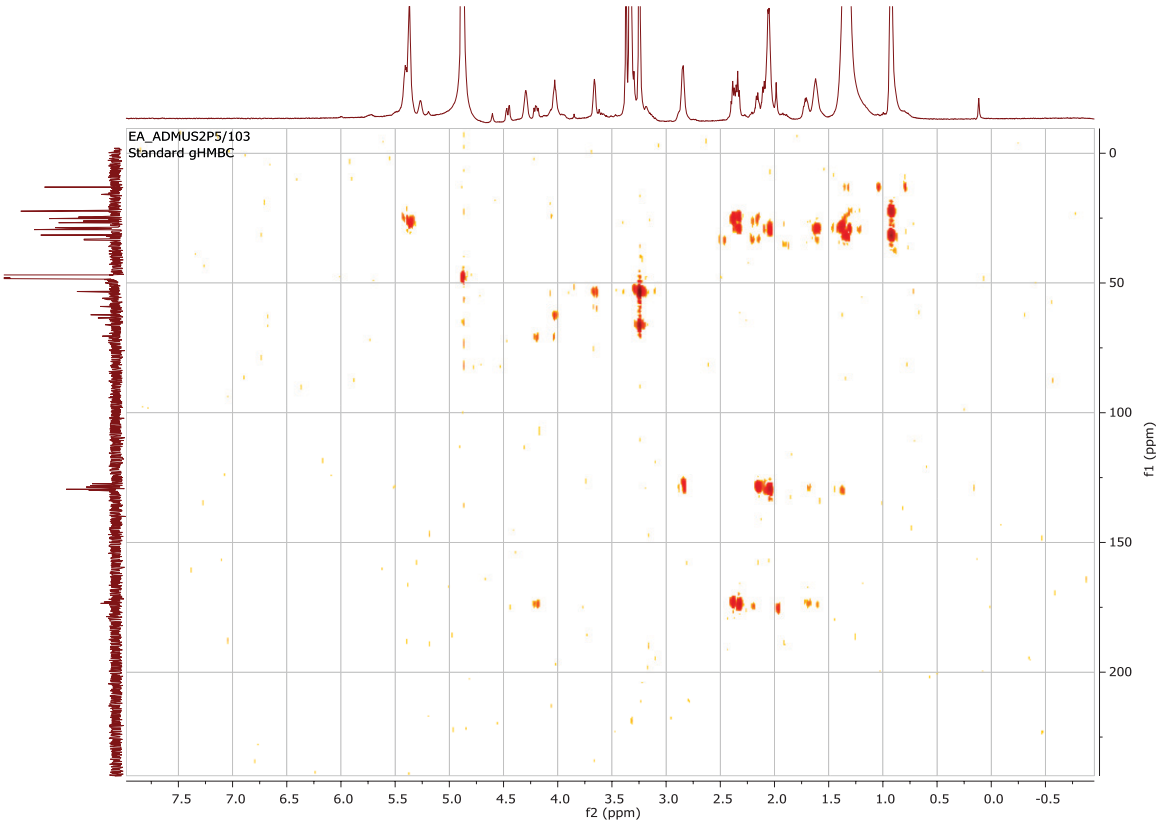

Figure A6. 600 MHz HMBC spectrum of bathymodiolamide C (1) in CD_3OD.

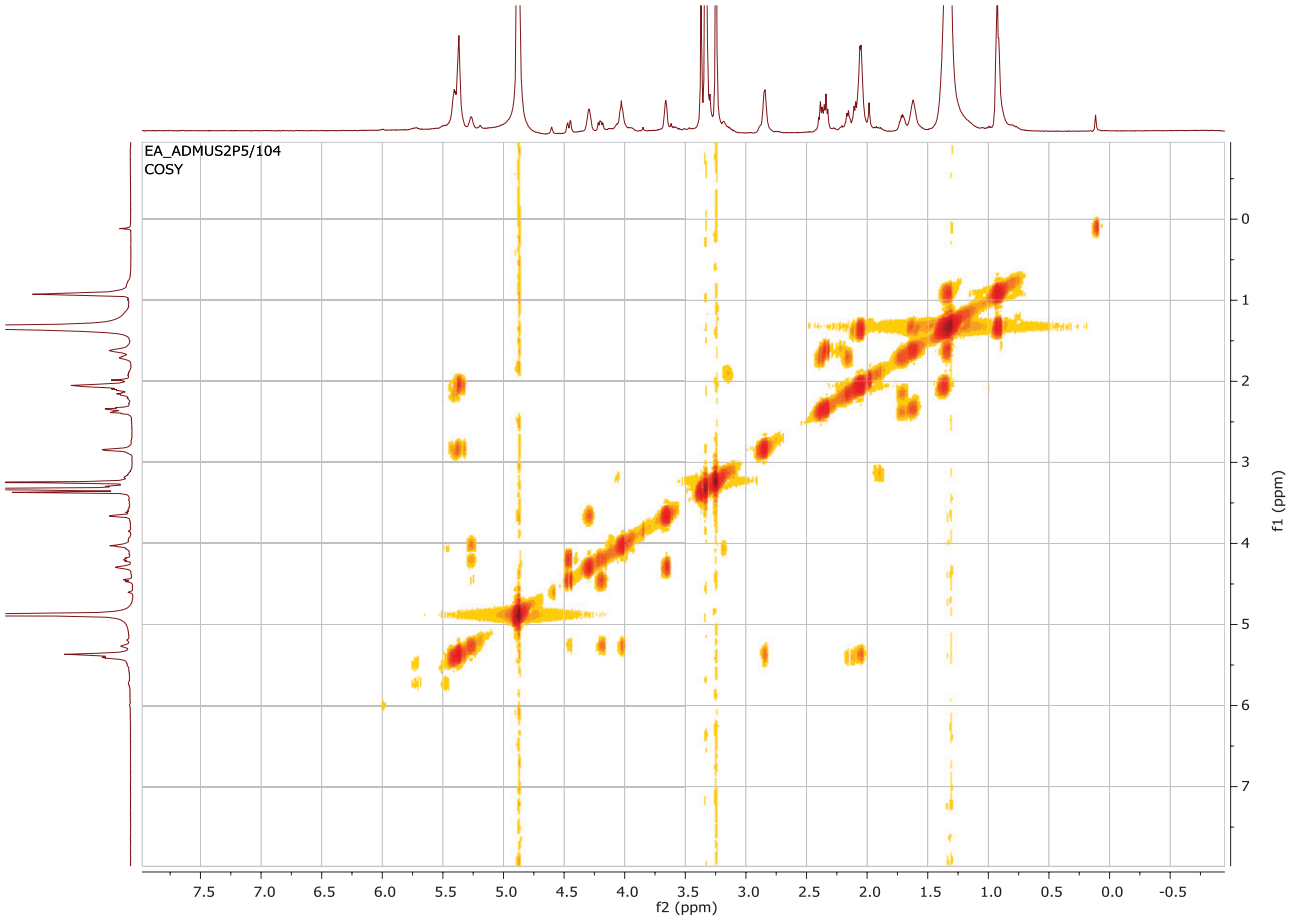

Figure A7. 600 MHz COSY spectrum of bathymodiolamide C (1) in CD_3OD.

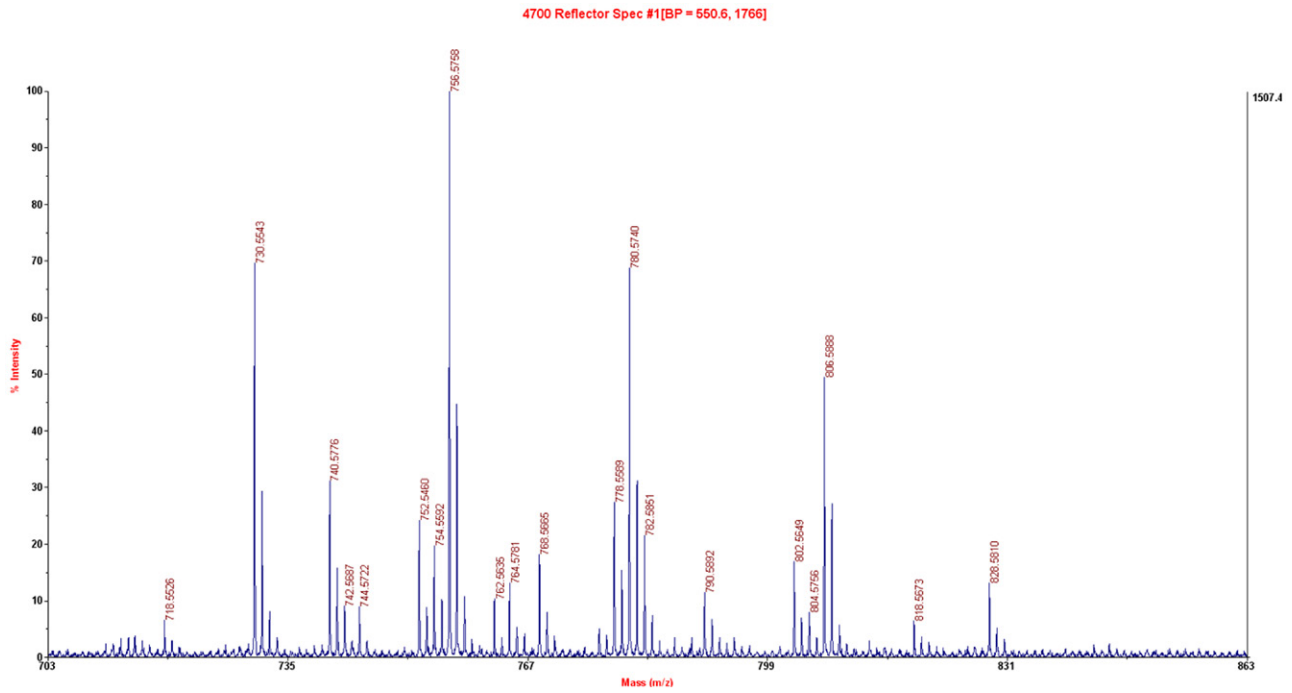

Figure A8. MALDITOFMS of bathymodiolamide D (2).

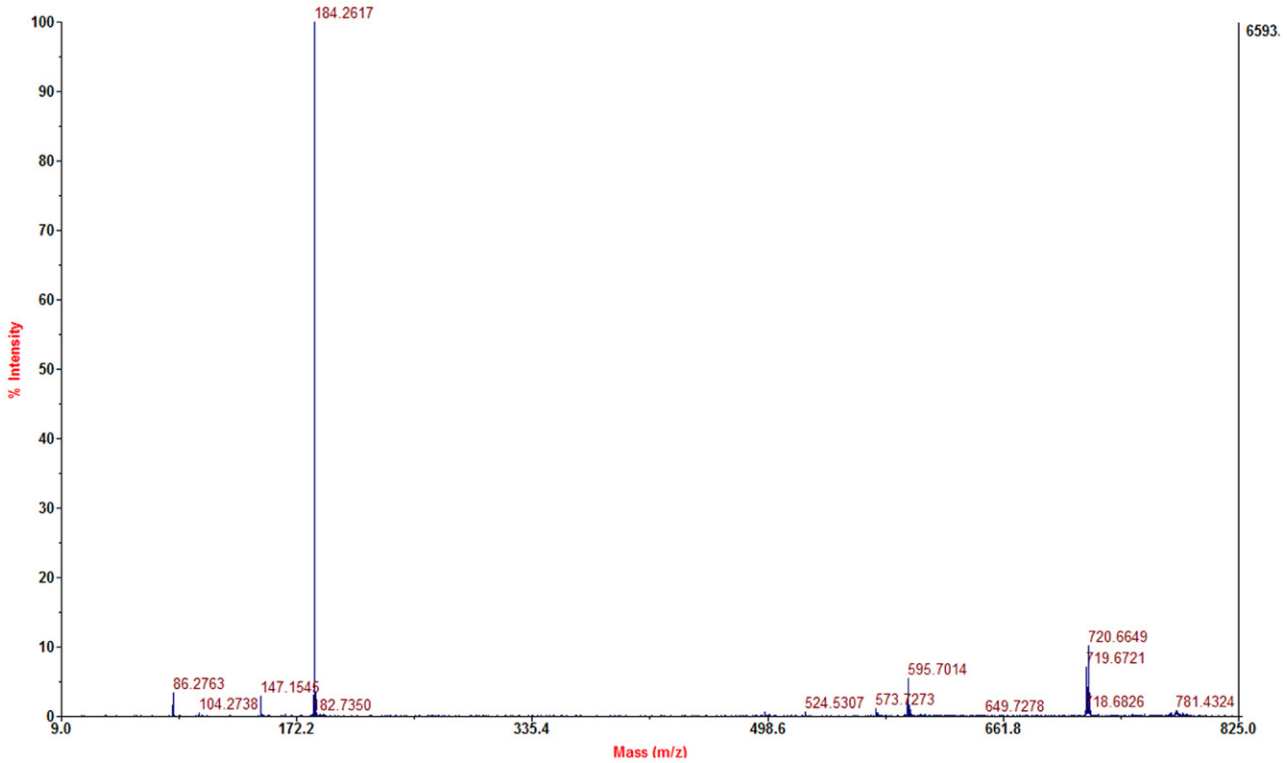

Figure A9. MALDITOFMS/MS of the peak at *m/z* 780.6 of bathymodiolamide D (2).

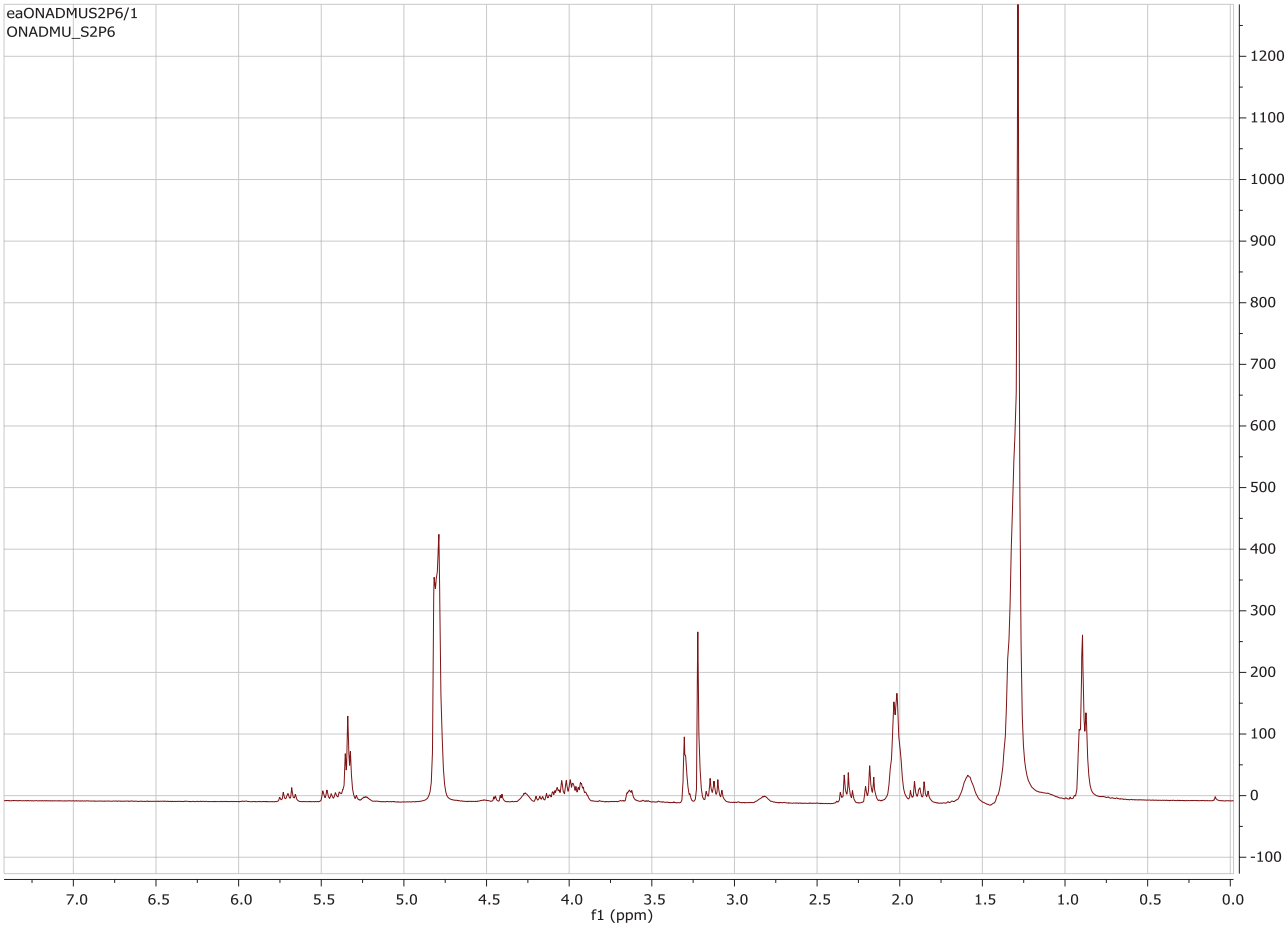

Figure A10. 600 MHz ^{1}H NMR spectrum of bathymodiolamide D (2) in CD_3OD.

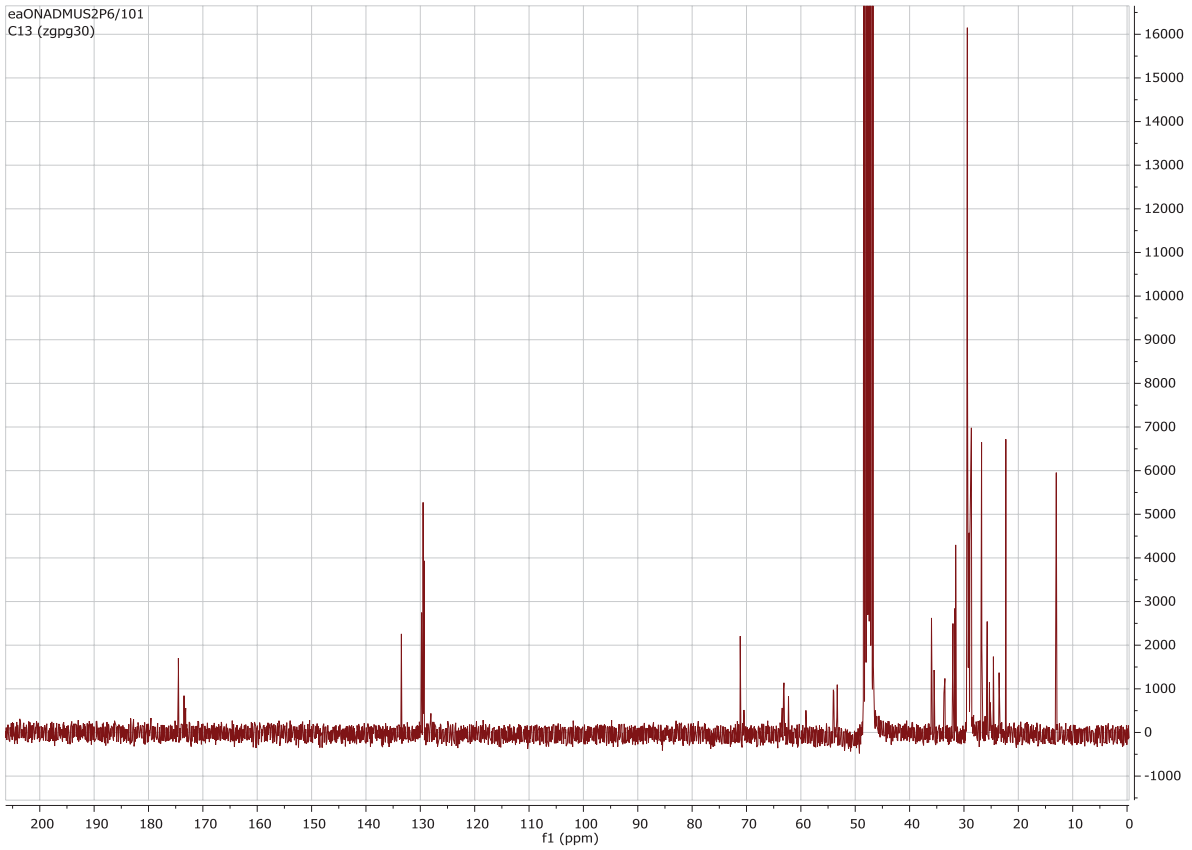

Figure A11. 150 MHz ^{13}C NMR spectrum of bathymodiolamide D (2) in CD_3OD.

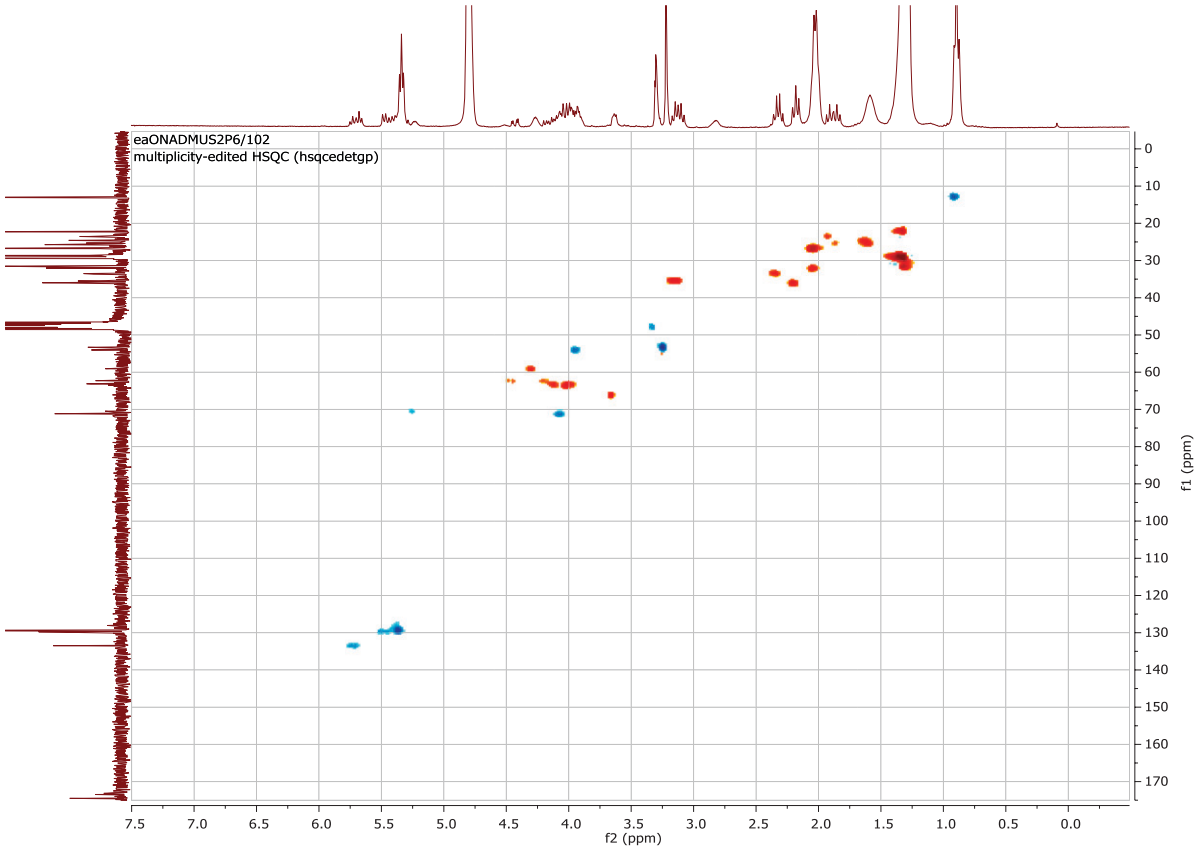

Figure A12. 600 MHz multiplicity edited HSQC spectrum of bathymodiolamide D (2) in CD_3OD.

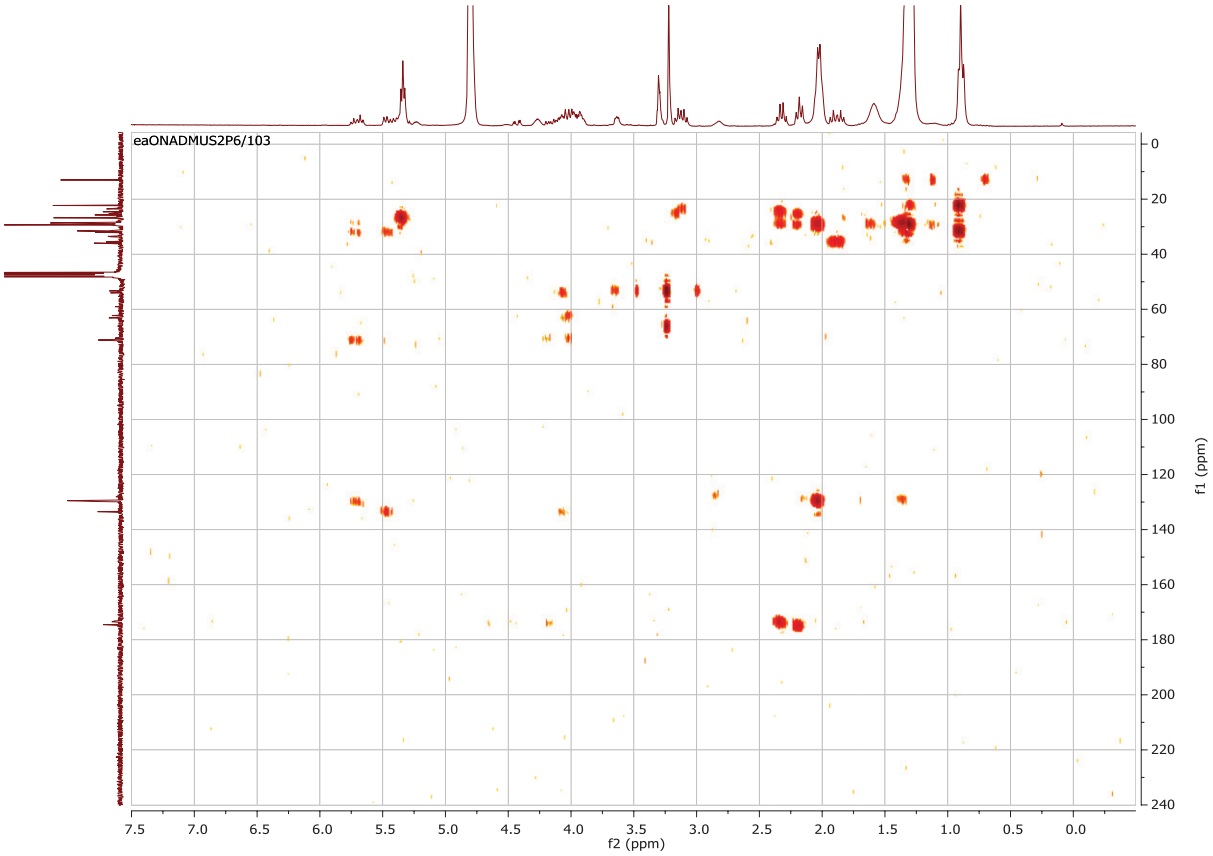

Figure A13. 600 MHz HMBC spectrum of bathymodiolamide D (2) in CD_3OD.

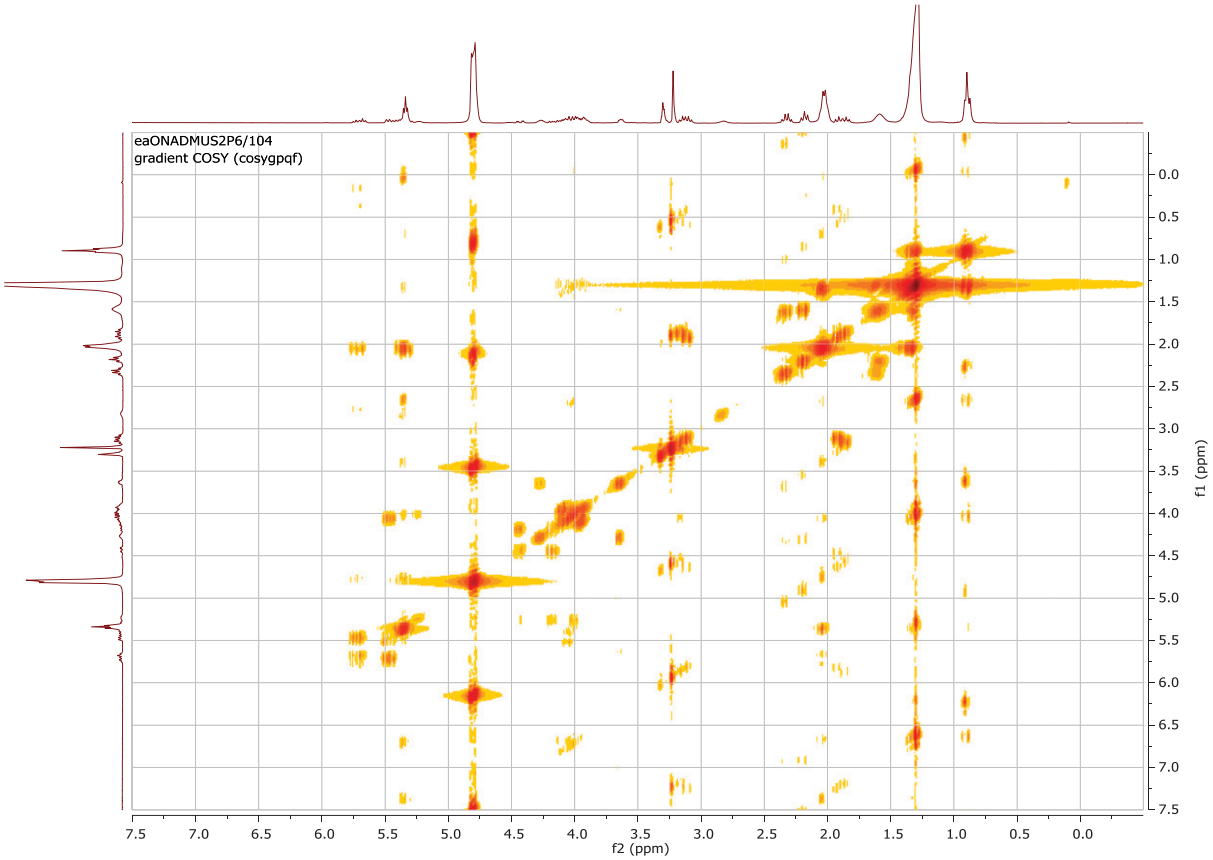

Figure A14. 600 MHz COSY spectrum of bathymodiolamide D (2) in CD_3OD.

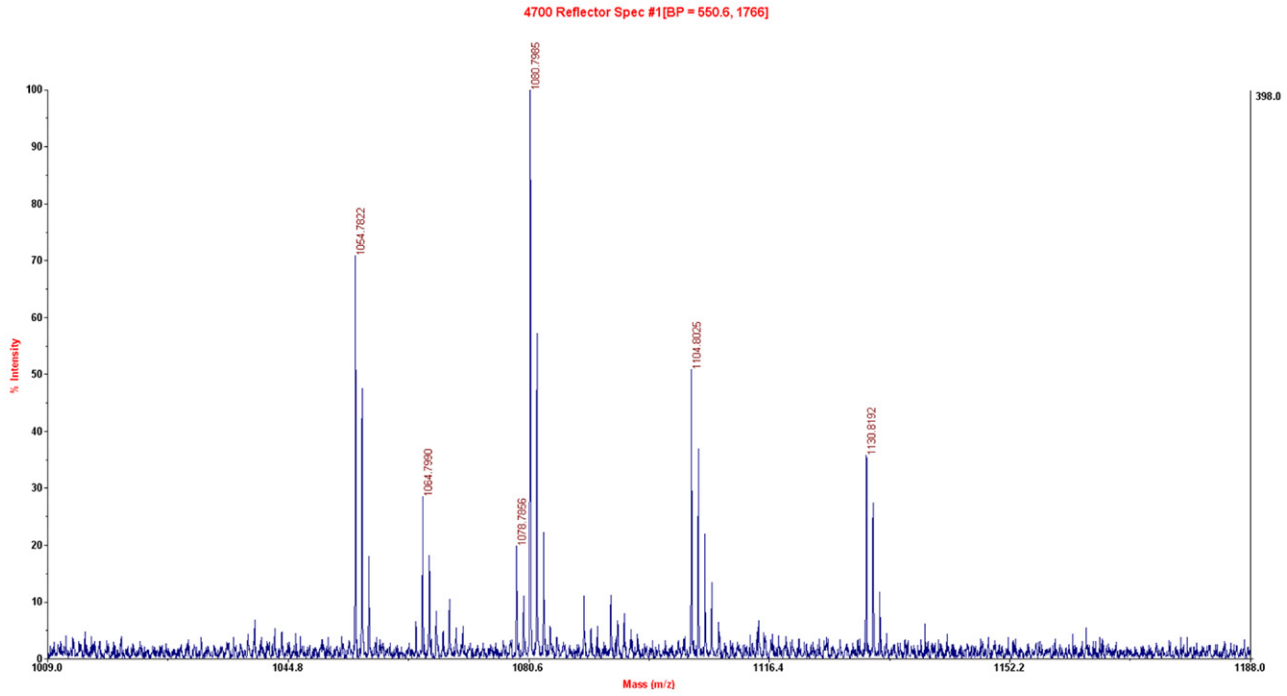

Figure A15. MALDITOFMS of bathymodiolamide C (3).

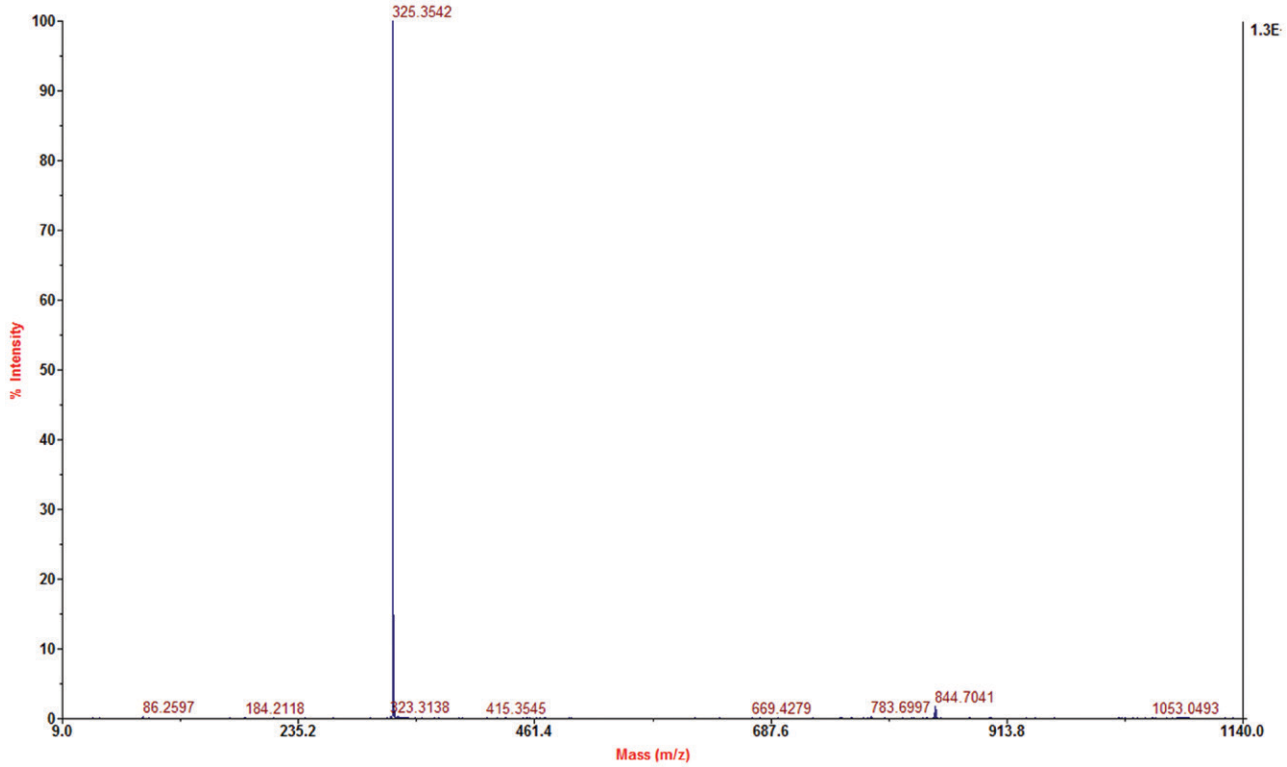

Figure A16. MALDITOFMS/MS of the peak at *m/z* 1,080.8 of bathymodiolamide D (3).

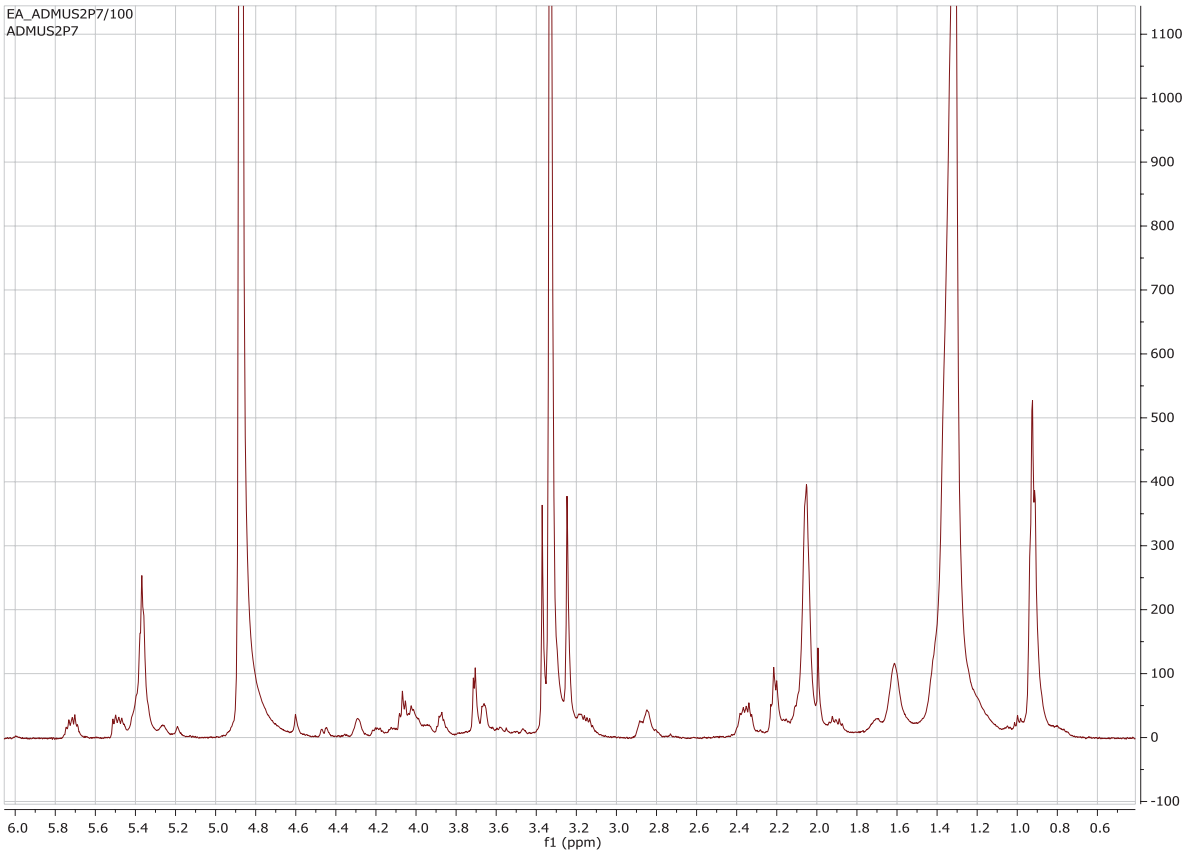

Figure A17. 600 MHz ^{1}H NMR spectrum of bathymodiolamide E (3) in CD_3OD.

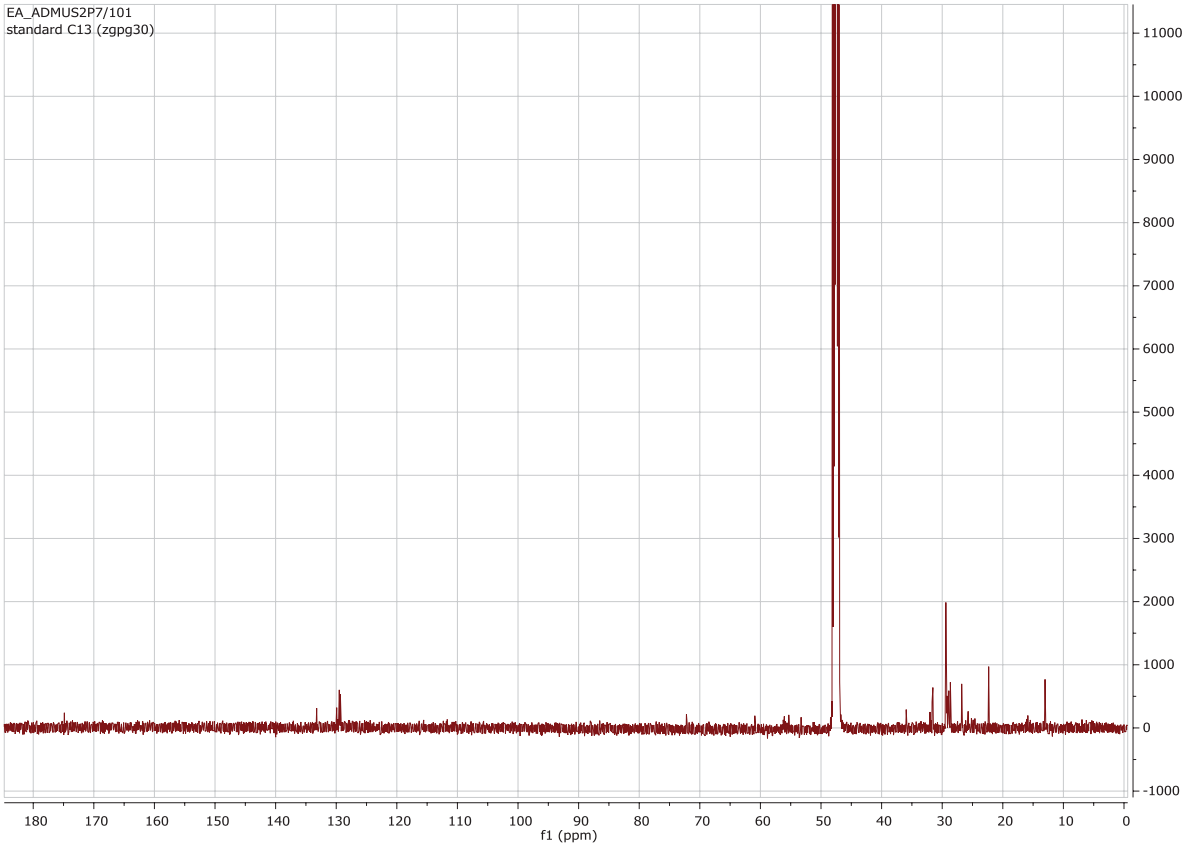

Figure A18. 150 MHz ^{13}C NMR spectrum of bathymodiolamide E (3) in CD_3OD.

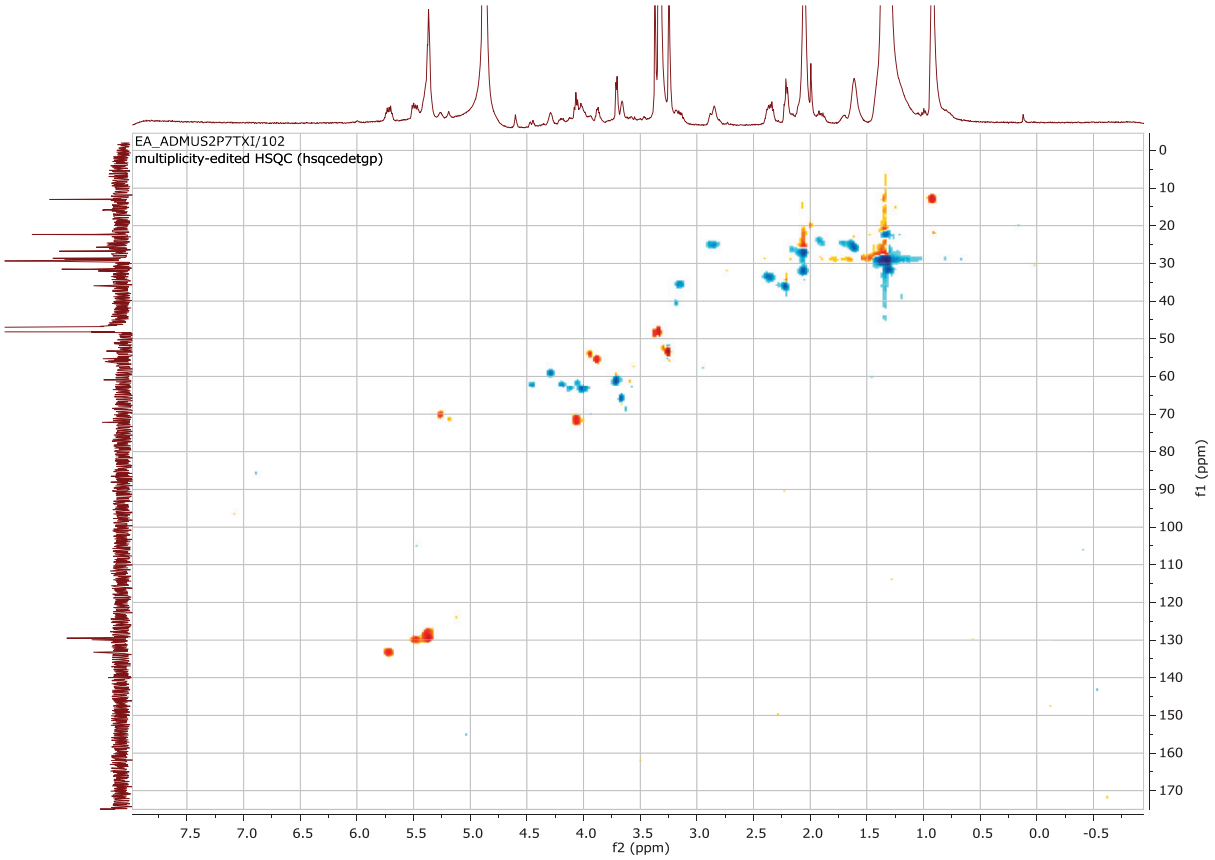

Figure A19. 600 MHz multiplicity edited HSQC spectrum of bathymodiolamide E (3) in CD_3OD.

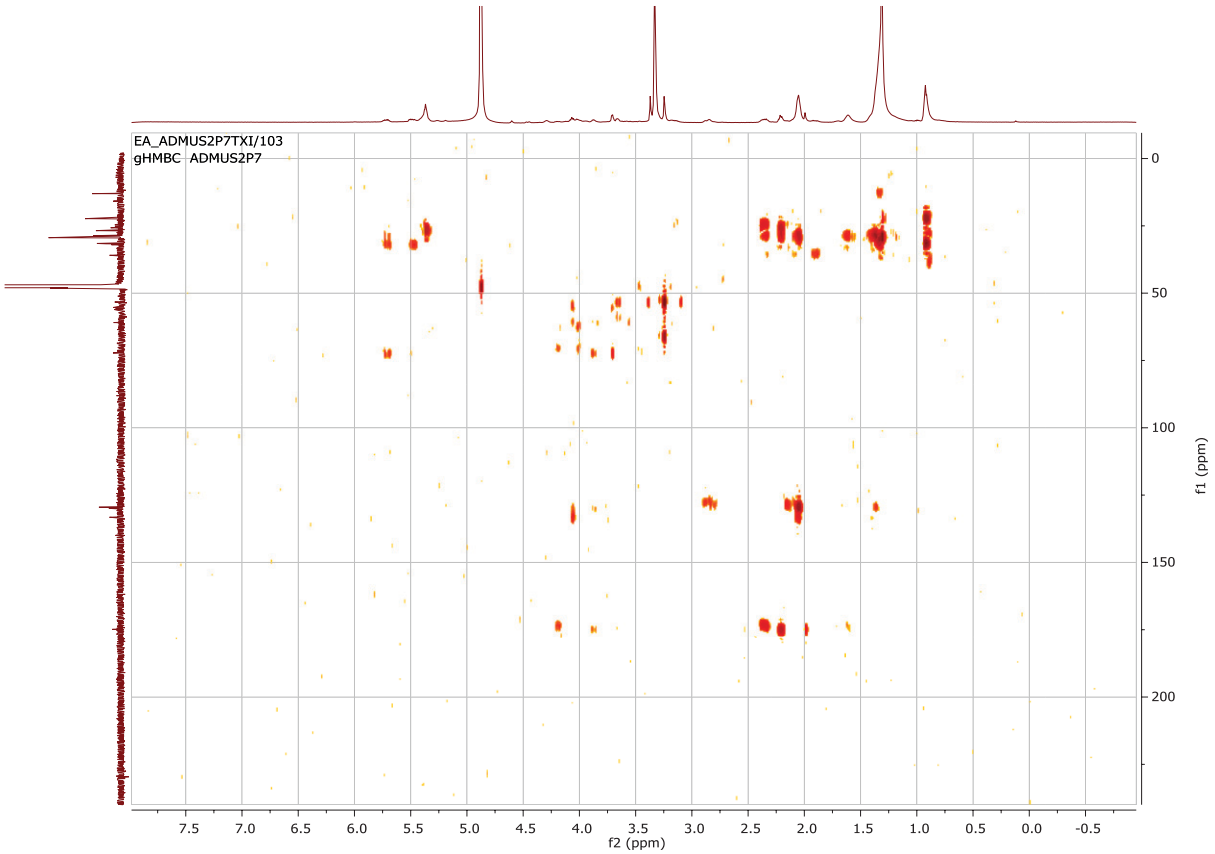

Figure A20. 600 MHz HMBC spectrum of bathymodiolamide E (3) in CD_3OD.

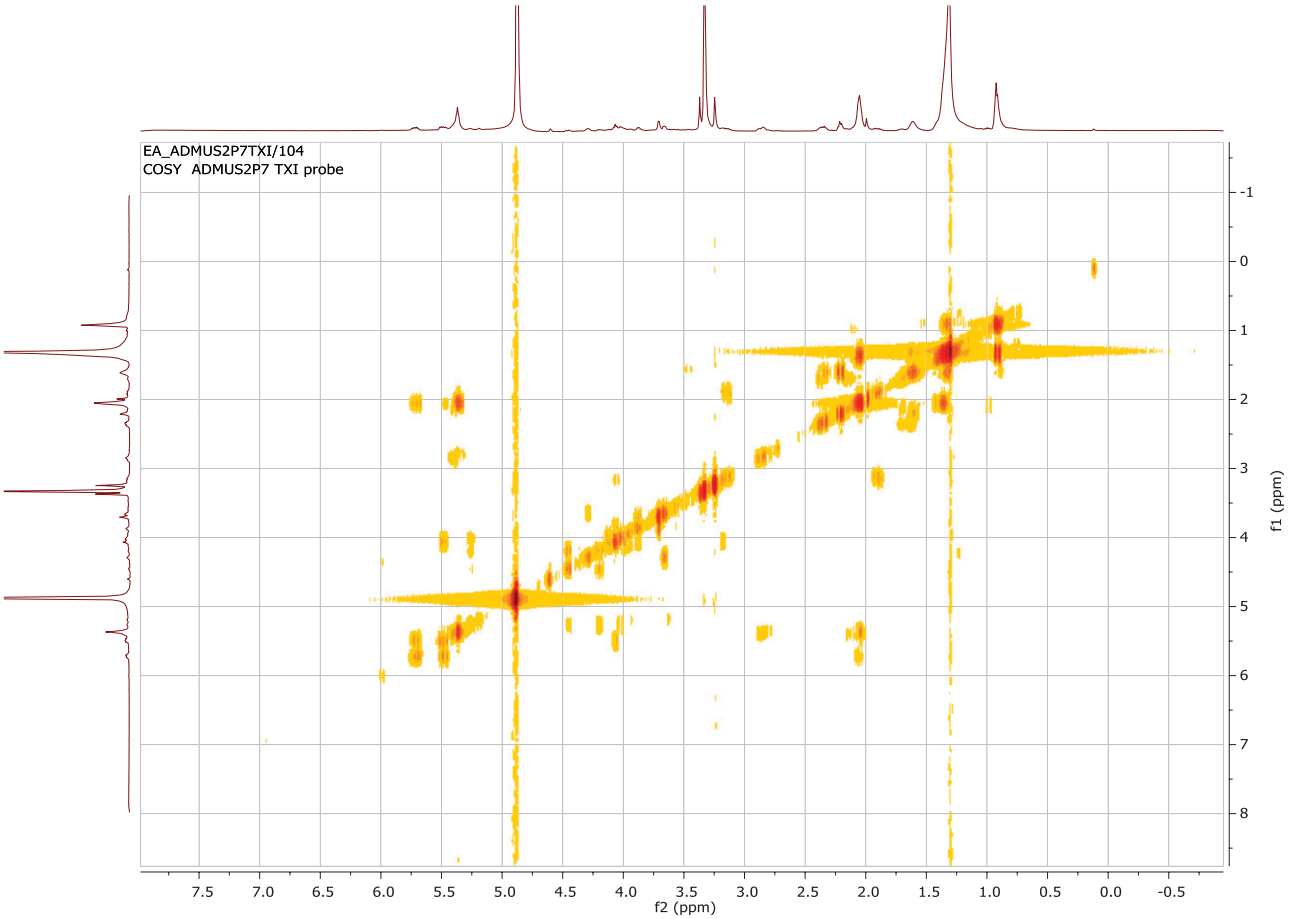

Figure A21. 600 MHz COSY spectrum of bathymodiolamide E (3) in CD_3OD.